Analysis of Channel Measurements Using a Very Large Antenna Array

Tomas Sidabras
Mohammad Salman

Department of Electrical and Information Technology
Lund University

Advisor: Ghassan Dahman

November 25, 2015

Printed in Sweden
E-huset, Lund, 2015

Acknowledgements

We are very thankful to our supervisor Dr. Ghassan Dahman for continuous support, motivation, patience and professional guidance throughout all stages of this thesis study. Moreover, we are grateful for his help and assistance during the several overnight measurement sessions.

We would also like to thank department of Electrical and Information Technology and Prof. Fredrik Tufvesson for offering a chance to perform this measurement campaign as our master thesis project. Working on this project helped us to better understand concept of channel modeling.

Tomas Sidabras would also like to express his appreciation to his parents and his sister for endless support and encouragement.

Tomas Sidabras
Mohammad Salman

Preface

This thesis was carried out by Tomas Sidabras and Mohammad Salman in collaboration with advisor Dr. Ghassan Dahman. Both Tomas and Mohammad were pursuing the same goal — study the effect of frequency, antenna polarisation and antenna directivity on channel behavior. Therefore, both authors were involved in all parts of the thesis work and it is hard to separate individual efforts.

Abstract

Accurate wireless channel models are crucial to simulate the effect of radio wave propagation in a channel on wireless communication systems. By calculating physical processing effects that signal undergoes while traveling from transmitter to the receiver, channel models help to analyze performance of wireless systems. State of the art channel model such as WINNER and COST 2100 are able to model the characteristics of conventional MIMO (Multiple-Input Multiple-Output) systems (where moderate number of antennas is used at the two sides of the link) with sufficient accuracy. However, model extensions are needed for the current models in order to be able to capture new propagation characteristics result from having massive number of antenna elements at one or both ends of the communication link. In this thesis work, a measurement campaign is performed using very large antenna array (about 7.5m long) in order to study key propagation characteristics for massive MIMO. The channel measurements are performed using two frequency bands (2.6 GHz and 5.1 GHz), vertical and horizontal antenna polarizations, directional and omni-directional antennas. Effect of aforementioned setup parameters on cluster delay and angle spreads, power slope and shadowing, number of clusters and their observation lengths are studied in this work. Also correlation among estimated cluster parameters is presented. It was observed, that antenna polarization does not have significant effect on estimated cluster parameters. On the other hand, some estimated parameters like delay and angle spread, shadowing achieve higher values using 2.6 GHz band. Impact of antenna directivity was not very significant. Results of this thesis work are important while implementing extension for cluster-based COST 2100 channel model for massive MIMO case.

Table of Contents

List of Figures

List of Tables

List of abbreviations

AoA	Angle-of-Arrival
AoD	Angle-of-Departure
BS	Base Station
BS-VR	Base Station Visibility Region
CBSM	Correlation Based Stochastic Channel Model
CDF	Cumulative Distribution Function
CSI	Channel State Information
CVI	Cluster Validity Index
DoF	Degree of Freedom
DMC	Dense Multipath Components
EM	Expectation Maximization
FDD	Frequency Division-Duplex
GSCM	Geometry Based Stochastic Channel Model
IO	Interacting Object
IRES	Impulse Response Estimates
ISI	Inter Symbol Interference
LOS	Line of Sight
LTE	Long-Term Evolution
MCD	Multipath Component Distance
MIMO	Multiple-Input Multiple-Output
MU-MIMO	Multiuser Multiple-Input Multiple-Output
MUSIC	Multiple Signal Classification
MPC	Multipath Component
MR-DMS	Multi-reference detection of Maximum Separation
MS	Mobile Station
MS-VR	Mobile Station Visibility Region
NLOS	Non-Line of sight
PDP	Power Delay Profile

RF	Radio Frequency
RX	Receiver
SAGE	Space-Alternating Generalized Expectation-Maximization
SIC	Successive Interference Cancellation
SIMO	Single-Input Multiple-Output
SNR	Signal to Noise Ratio
TDD	Time Division-Duplex
TEM	Transverse Electromagnetic Wave
TX	Transmitter
UE	User Equipment
VNA	Vector Network Analyzer
VR	Visibility Region
WDCM	Wideband Directional Channel Model
WSS	Wide-Sense Stationary
XPD	Cross-Polarization Discrimination

Chapter 1

Introduction

With the increasing demand of wireless connectivity and high throughput, advanced wireless technologies have to be implemented to meet these demands. Multiple antenna systems (MIMO) integrated in wireless standards like 4G LTE (Long-Term Evolution) increase link efficiency compared to single antenna systems. Equipping transmitter and receiver with multiple antennas significantly enhances wireless system performance. Conventional MIMO systems with up to 8 antennas are becoming mature and new solutions have to be presented for better performance. Recently, massive MIMO systems equipped with large amounts of antennas (hundreds or thousands) have been introduced. It has been shown in theory that massive MIMO can deliver higher data rates and link reliability, better exploit of propagation channel with higher spatial resolution. A high degree of freedom added by a large number of antennas can allow system to focus the field strength to a specific geographical point improving radiated energy efficiency [1], [2]. It has been shown that massive MIMO delivers favorable characteristics for efficient system performance in real propagation environments during few measurement campaigns [3], [4], [5]–[7]. However, more channel measurements are required in order to supplement theoretical studies and collect enough data for developing accurate channel models for systems with very large antenna arrays. The first measurement-based channel modeling effort for very large antenna arrays was done in [5] proposing new parameters for an extension to cluster-based COST 2100 channel model. In [5] behavior of delay and angle spread of cluster, cluster visibility region at base station (BS) side, statistics of power and length were introduced. However, more measurements are still needed in order to gather the information required in order to be able to extend the current COST 2100 model to the massive MIMO case.

1.1 Thesis aim

For this thesis project, two channel measurement campaigns were performed with an aim to study effect of frequency band, antenna polarization and antenna directivity on the behavior of channels with very large antenna array. During the measurements, array at base station was used with 128 antenna elements and 256 antenna elements for 2.6 GHz band and 5.1 GHz band, respectively. Three different antenna setups were employed — directional at transmitter and receiver, omni-diredctional at transmitter and receiver, omni-directional at transmitter and directional at receiver.

From the collected measurement data extracted multipath components (MPCs) grouped into clusters are related to interacting objects (IOs) between transmitter and receiver. The impact of different setup parameters (frequency band, antenna polarization and directivity) on identified cluster characteristics — angle and delay spreads, power slope and shadowing, correlation among parameters — is studied with an aim to provide a comparison of characteristics and give ability to develop statistical models for them.

1.2 Organization of thesis

This thesis is organized as follows:

- Background information related to the thesis is presented in Chapter 2;
- Measurement setup and parameters, measurement area are described in Chapter 3;
- Chapter 4 presents cluster identification methods, cluster parameters estimation;
- Measurement data analysis is presented in Chapter 5;
- Chapter 6 concludes the thesis work findings and proposes future work.

Chapter 2

Background information: Multiple-Input Multiple-Output Radio Wave Propagation

In this chapter we describe the background information, which is relevant for the thesis. We start by describing radio wave propagation and some of their characteristics. It is followed by description of antennas and their parameters and introduction to the Multiple-Input Multiple-Output (MIMO) antenna systems and MIMO channel models. After that, massive MIMO systems are introduced together with their corresponding channel models. Finally, different measurement campaigns as well as theoretical studies for massive MIMO investigation are presented at the end of this chapter.

2.1 Radio wave propagation

In wireless communication systems, radio waves travel from transmitter to receiver through medium, i.e. air, known as a radio channel. Signal sent from transmitter can reach receiver directly in line-of-sight communication (LOS) or via a number of many different indirect propagation paths as a result of three main propagation mechanisms — reflection, diffraction, scattering. The latter case is referred to as non-line-of-sight (NLOS) communication, where different interacting objects in the propagation environment — for example, buildings, mountains, trees, etc, block the direct signal between the transmitter and the receiver. If radio wave is interacting with IOs, which have smooth surfaces (compared to the dimension of the wavelength), waves are reflected and some of the wave energy penetrates the IOs. If the surface of IO is rough (compared to the dimension of the wavelength), the wave is scattered. Wave diffraction can appear at the edges of IO, i.e. corner of the building. Depending on the complexity of the environment, the number of propagation paths may vary. If the environment is rich with IOs, the number of possible propagation paths can be very large. Delayed and attenuated versions of original transmitted signal traveling through these propagation paths are known as multipath components and each of them can be characterized by several parameters among which is: propagation delay, angle-of-arrival (AoA) and complex amplitude [8].

Normally simple receiver cannot distinguish among different MPCs and just adds all of them up. This results in combining a number of MPCs, which can

be destructive or constructive depending on their phases. In case of destructive combining, the amplitude of the received signal can drop significantly — the signal fading process is observed. This can be usually experienced when the transmitter (TX), receiver (RX) or IOs are moving so that the phase of each MPC differs, as well as delay. This can also influence angles of arrival of MPCs [8].

2.2 Antennas

Performance of wireless systems is greatly affected by antennas and their characteristics (e.g. polarization, radiation pattern) as well as by the number of antennas used. In radio and microwave frequency bands, antenna can be described as part of transmitting or receiving system designed to radiate electromagnetic waves into particular beam width or receive radiated electromagnetic waves. Antenna converts power into electromagnetic waves. If possible, the transmitted signal is directed in a way that interference with other propagated signals at the same frequency band is minimum and signal to noise ratio (SNR) at the receiver side is maximum. Electromagnetic waves are considered to normally propagate in a way that electric field and magnetic field are not perpendicular to the propagation direction. This characterizes a transverse electromagnetic wave (TEM). In the TEM wave electric field E can be chosen to radiate in z axis direction and magnetic field H in x axis direction so that the direction of the TEM wave propagation is in y axis direction. TEM wave is shown in Figure 2.1 [9].

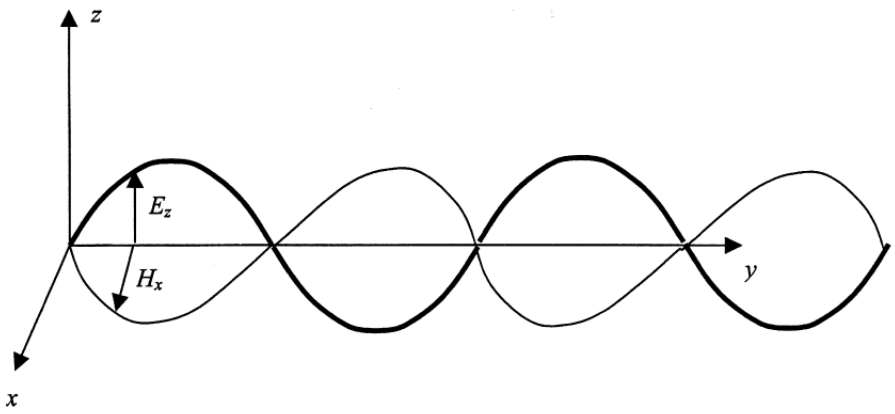

Figure 2.1: Electromagnetic wave [9].

Characteristics of receiving antennas are identical to transmitting antennas — receiving and transmitting antennas can be exchanged without signal strength decrease at the receiver. Radiation directivity and polarization are the most important antenna characteristics, which have to be considered when designing the wireless communication system in order to achieve the highest efficiency [9].

According to application (e.g. broadcast, point-to-point, etc.), environment (e.g. rural area, urban area with buildings of different height) there are different

requirements for antenna systems. Broadcast applications require a wide angle of radiation over a large area whereas in point-to-point applications power should be radiated in a small angle. Therefore, a sufficient radiation directivity for a particular application is the requirement that should be met when designing communication systems. Directional characteristics of antenna can be described in radiation pattern, which can be two or three dimensional. Radiation pattern defines relative signal strength as a function of an angle. A pattern is isotropic if the radiation is the same in all directions. Omni-directional antennas describe antennas with an isotropic radiation pattern in a single plane. On the contrary, directional antennas have no symmetry in the radiation pattern. Main lobe in the pattern defines the direction where the power is radiated or received and it is surrounded by several times smaller side lobes with relatively weaker radiation [9].

Desired antenna radiation pattern is different for base stations (BS) and mobile stations (MS) [8]. Knowing the position and orientation of BS antenna, its radiation pattern should be shaped in a way that energy is not wasted. In certain types of terrain, omni-directional antennas might be used to improve signal transmission and reception. In metropolitan area, omni-directional antennas can be situated on the roof of the building in order to communicate with more than one station around that area. When mounted with respect to the ceiling, omni-directional antennas can also cover intended indoors area. Directional antennas focus energy in a particular direction. Thus, they can be employed in the base station applications where a specific sector has to be covered by a separate antenna [9].

The polarization of an antenna can be defined by the plane in which electric wave vibrates. In a linear polarization category it can be horizontal or vertical. If electric field radiates in z axis direction, polarization is vertical and if electric fields radiates in x axis direction, polarization is considered horizontal. Antennas are highly sensitive to polarization, therefore, it is essential to match the polarization of all communicating radio frequency antennas in the wireless system. Not matching transmitting and receiving antenna polarization results in a decreased level of received signal strength. The polarization of the electromagnetic wave might slightly change during transmission due to the scattering path but it will remain broadly the same [9].

Cross-polarization is known as an orthogonal radiation of desired polarization of wave. A proportion of the signal, which is transmitted in orthogonal polarization than it was required is defined by cross-polarization discrimination (XPD) [10].

2.3 Multiple-Input Multiple-Output Systems

Meeting radiation directivity requirements for specific application or properly utilizing antenna polarization may help to prevent the significant loss of signal strength. However, a certain service quality level guaranteeing reliable high data rate communication can no longer be delivered by conventional single-antenna wireless technologies. The number of individual wireless connections is increasing everyday requiring robust communication with low error probability and higher

data rates than ever before. Therefore, additional methods are needed for improving the wireless links and meeting the new demanded requirements.

Fading process can be mitigated and angular spread can be exploited in more complex receivers, which contain more than one antenna. Such receivers can distinguish MPCs with different AoAs, process them separately and in this way reduce the fading. Even better system performance can be achieved when multiple antennas are employed at both system ends — TX and RX. These systems that are called MIMO (Multiple-Input Multiple-Output) can offer interference suppression, beamforming, diversity and spatial multiplexing. MIMO enables bit rate enhancement, better bit error performance, higher signal to noise ratio for wireless systems [8].

Compared to conventional single-antenna systems, MIMO technology can deliver higher bit-rates utilizing same fixed bandwidth and without increase in transmit power. Bit rate can be enhanced several times depending on the number of antennas used. This is achieved by a spatial multiplexing technique — when the independent information is transmitted over the radio channel simultaneously by each antenna in use. Transmitted individual signals are superimposed over the propagation channel but with the use of several antennas at the receiver and interference cancellation sort of algorithm signals are separated again. The increase of bit-rate because of the spatial multiplexing is called a multiplexing gain [8].

MIMO technology also increases signal to noise ratio at the receiver by utilizing adaptive antenna arrays. Radiation patterns of multiple antennas at receiver and transmitter can be steered in the desired direction, avoiding unwanted directions with interference. This beamforming technique brings gains in SNR that are known as array or antenna gain [8].

MIMO can be used in wireless systems to communicate with several terminals simultaneously. All MIMO improvements over use of single antenna can be delivered to each terminal and the more antennas are used, the more independent data streams can be created reaching more terminals at the same time. This technology is known as multiuser MIMO (MU-MIMO) and is adopted in modern wireless broadband standards like 4G LTE. However, recent standards like LTE-Advanced using MU-MIMO employs only up to 8 antennas at the base station and the overall improvement is still relatively modest [2].

2.4 MIMO Channel Models

Channel models are of a great importance during development of wireless systems for identifying optimum site parameters, analyzing system performance, and efficient signal processing. Channel models may be of two main classes — deterministic and stochastic. Deterministic channel models are based on very accurate and thorough description of a real-life environment. On the other hand, radio wave propagation channel is described indirectly in stochastic channel models — environment is reflected based on statistical means. However, stochastic channel models have to reproduce all effects that have impact on the propagation so that the simulation scenario would be as close to reality as possible. Recorded impulse response and Ray-tracing technique are of deterministic channel model

class. Geometrically-based, parametric, correlation-based channel model belong to stochastic channel models[11].

For MIMO system design and evaluation small-scale fading MIMO channel models are implemented. Geometry-based stochastic channel models (GSCM) like one-ring, two-ring, ellipse, COST 2100 models and correlation based stochastic channel models (CBSM) like Kronecker and Weichselber models are used for conventional MIMO system investigation [11],[14].

2.4.1 Correlation Based Stochastic Channel Model

It is assumed that spatial correlation among antennas results from the scattering in their closest surrounding areas. Whereas, correlation between two propagation paths is a result of the correlation between antennas at transmitter and receiver sides connected by these paths. Correlation among receiving antennas is independent of transmitting antennas and correlation properties among transmitting antennas is independent of receiving antennas [11].

Correlation Based Stochastic Channel Model notes the correlation at both link ends (as it is done in Kronecker CBSM model) and models their mutual dependence (as it is done in virtual channel representation) [12]. It is assumed [13] that spatial correlation at the transmitter and receiver do not depend on the number of transmit antennas and receive antennas respectively.

Correlation Based Stochastic Channel model has lower complexity than Geometry Based Stochastic Channel Model but at the same time it has lower accuracy. This is not acceptable while modeling non-stationary channel with the use of spherical wave effect and for more reliable modeling [11].

2.4.2 Geometry Based Stochastic Channel Model

Geometry-based Stochastic Channel Model is a model, which reproduces the stochastic properties of MIMO channels over frequency, time and space using stochastic geometrical distribution of scatterers. The ability of cluster-based GSCM to model time and spatially variant models is an important reason that such widely used channel models like WINNER and COST2100 are based on the concept of GSCM. GSCM delivers angular characteristics of radio waves and it can be used for creating channel responses for different environments for indoor and outdoor propagation [14].

In extended GSCM for base stations with antenna arrays a number of mobile stations are in the visibility region of one or several arrays at a time. Both mobile stations and base stations are surrounded by scatterers that cause specular reflections. The signal path starts at the transmitter and after reflection from one or several scatterers it ends at the receiver. Several scatterers form a cluster where all scatterers hold same long term properties [14].

Clusters in this model contain closely positioned multipath propagation components (MPCs) where each MPC represent the different path between the transmitting and receiving antenna elements. Based on geometry of the propagation environment each MPC can be described by a number of parameters. In

the GSCM channel model is obtained based on positions of scatterers by applying laws of specular reflection, diffraction and scattering [11] [15].

Geometry based stochastic channel model is adjusted in other channel models basing on particular GSCM parameters, extending parameters or incorporating new parameters in the model. There is a number of channel models based on GSCM. A Wideband Directional Channel Model (WDCM) is designed for micro and macro cells where distribution area of scatterers follows a Gaussian distribution and is circular or elliptical. The WDCM as well as most of the GSCMs are single bounce models that consider only single specular reflection. COST 273 and WINNER models use the concept of clusters containing multipath components with similar parameters representing each link between transmitter and receiver. A COST 259 model can be used for micro and macro cellular environments where scatterers are placed around base and mobile stations. Additional scatterers are placed around the base station in micro cell environment. However, this is not applied for macro cell environments because of their exposed positions above the rooftop [14]. A COST 2100 channel model is widely used GSCM since this model supports non-stationary phenomena and unceasing evolution of radio channel. Current COST 2100 channel model takes in consideration visibility region at the user equipment side. However, new measurements [5] extend visibility region concept also to the base station side.

2.5 Massive MIMO Systems

Massive multiple-input multiple-output is an emerging technology, which is able to deliver all benefits of MIMO but on a much greater scale. Instead of 8 antennas, massive MIMO can use hundreds of antennas serving a great number of terminals utilizing the same time-frequency resource. There are many different configurations and deployment possibilities of hundreds of service antennas and some of them are depicted in Figure 2.2 [2].

Having a large number of antennas at the base station brings various benefits to the wireless systems like the low cost of manufacturing: antennas for massive MIMO can be built using inexpensive, low-power components. For instance, several high power amplifiers can be substituted by hundreds of low-cost amplifiers and bulky coaxial cables can be eliminated. Massive MU-MIMO can significantly increase energy-efficiency as large number of antennas can focus energy to a small area. When the number of serving antennas exceeds number of terminals there is a high degree of freedom (DoF), which can be used for signal shaping. Massive MIMO ability to operate with reduced amount of power is significant as the energy consumption in base stations is of great importance for economic and ecological reasons. Several times higher spectral efficiency can be achieved when serving many terminals at the same time in the same time-frequency resource. Having the high degree of freedom can also serve by cancelling unwanted or intentional jamming signals and in this way enhancing system robustness [2].

Conventional systems send data streams to users via different times (time-division multiplexing) or using different frequencies (frequency-division multiplexing). In massive MIMO, different data streams utilize same time and frequency by

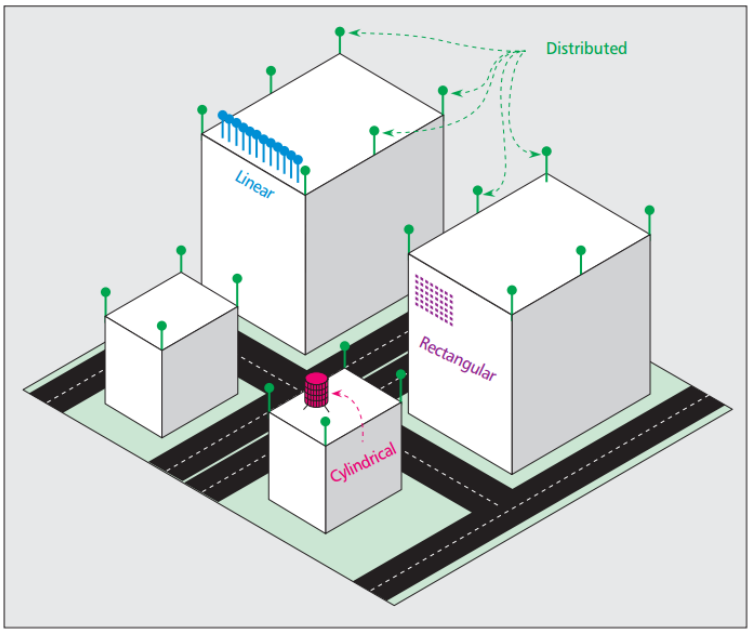

Figure 2.2: Massive MIMO antenna deployment possibilities [2].

using spatial multiplexing, which gives a significant increase in system capacity. However, this requires good channel knowledge that can be acquired by sending pilots from terminals for channel estimation in uplink. In downlink it is more complex situation since pilots for downlink estimation must be mutually orthogonal for all antennas which require more time-frequency resources the more antennas are used in base station. This relation also applies to the number of channel responses that becomes proportional to number of antennas. A time division-duplex (TDD) system can be used to solve the problem in the downlink case. With channel reciprocity assumption only channel state information (CSI) for the uplink estimation is enough. Base station can organize downlink transmission using the CSI acquired from the pilots, which are sent uplink by the terminals [2].

Massive MIMO can also sufficiently reduce latency in wireless communication systems. When the number of replicas of original signal travel from transmitter to receiver through many different paths in propagation environment some of the paths may undergo fading. If a terminal in communication occurs in a fading dip a channel has to change for terminal to emerge and be able to receive data again. This latency invoking fading is avoided in massive MIMO by the law of large numbers and beamforming techniques [2].

Massive MIMO promises significant improvements for modern wireless communication technologies but there are also some challenges and limitations that need to be attended. In multi-cellular systems pilot contamination creates signal interference as number of orthogonal pilot sequences is limited enforcing some terminals to use same pilot sequence. This interference grows with the number of service antennas. Massive MIMO requires simple but fast signal processing as

more antennas means more data. Power for baseband signal processing and overall consumed power has to be considered in order to be energy efficient. Low cost components results in higher hardware imperfections and phase noise. Channel models for conventional MIMO cannot be sufficiently used for massive MIMO for realistic performance evaluation as there are additional channel parameters that need to be considered. New models or extensions to existing models should be implemented for radio channel behavior studies [2].

2.6 Massive MIMO Channel Models

In order to properly investigate massive MIMO systems, new models or improvements and extensions to earlier described GSCM and CBSM channel models should be implemented. Channel models for conventional MIMO are not able to accurately evaluate some characteristics of massive MIMO. For instance, in conventional MIMO channel models it is assumed that the distance among receiving array and scatterers is far beyond Rayleigh — here far field distance and a plane wave front assumption can be applied. In massive MIMO system plane wave front assumption cannot be applied anymore due to the use of massive number of antennas in the array. Plane wave front model underestimates the massive MIMO system gain in some situations. A spherical wave channel model has to be used for massive MIMO investigation. Moreover cluster evolution on array axis has to be included in channel model. Because of a massive number of antennas an appearance and disappearance of clusters, angle-of-arrival shifts and non-stationaries can be experienced along the antenna array [11].

2.6.1 Extension of the COST 2100 Channel Model to Massive MIMO Channel

The COST 2100 model is a geometry based stochastic channel model based on geometrical distribution of clusters in the propagation environment. There are three types of clusters in COST 2100, which are depicted as ellipsoids in the space — that is local clusters situated around the BS or MS and far clusters, which can be single-bounce or multiple-bounce. Clustering of MPCs allows characterization of the large-scale channel properties (i.e., angle and delay spread, cluster attenuation and shadowing level) within each cluster [16].

Differently than in other models like WINNER II, clusters and their visibility regions stochastically represent physical environment, which is completely independent of the MS position. In COST 2100 it is considered that propagation channel is resolved into scatterers. Reflections from rough surfaces, corner diffractions can create diffuse scattering with significant contribution in delay and angular domains, which cannot be captured with few specular MPCs. Diffuse scattering is included in COST 2100 by a superposition of a large number of MPCs, which are called dense multipath components (DMCs), which contain modified delays, amplitudes and angles. When the number of DMCs is sufficiently large this method of MPC concept extension can capture the best residual channel spectrum [16].

COST 2100 channel model enables to fully characterize the behavior of stochastic channels in multi-link MIMO scenarios. A number of significant properties can be incorporated in the channel description and it is an essential approach for MIMO system channel estimation. However, more complex wireless communication systems like massive MIMO introduce new parameters that need to be considered. Therefore, extensions to COST 2100 as well as sufficient number of measurement campaigns are required to cover that [16]. There is a number of stochastic parameters defined for extension of COST 2100 model in theoretical studies and from channel measurements. One of them is cluster visibility region concept, which enables to determine visibility of each cluster. In the current COST 2100 model, visibility region is used only at the MS side whereas effect of spatially variant channel can be also experienced at the BS side when arrays with large number of antennas are used. Therefore, in extension for COST 2100 a visibility region is also defined for BS side [5].

2.6.2 Review of existing Massive MIMO channel measurement campaigns

Sufficient channel models are required in order to evaluate massive MIMO technology in realistic scenarios and to investigate the radio channel behavior. Several massive MIMO measurement campaigns were performed to supplement theoretical studies with investigation based on practical massive MIMO implementation. A number of channel characteristics are identified in measurement based studies that need to be implemented in new channel models for massive MIMO.

Measurements were performed in [17] to analyze propagation characteristics in outdoor environment. Main insight in these measurements was given into power levels, singular value distribution, antenna correlation, angular power spectrum and near-field effect. It was shown that large scale fading and a varying angular power spectrum may be observed over the large physical array. Angular power spectrum analysis displayed that far-field and wide-sense stationary (WSS) assumptions cannot be applied for such scale antenna array. Users in comparably stationary non-line of sight area undergo less varying correlation whereas users in line of sight exercise larger fluctuations leading to correlation variations. Correlation among users is low while using a large number of antennas. However, correlation coefficient decreases with decreasing number of antennas used due to decreasing independent channels. The measurements also propose the need of shadowing process utilization in base station for dealing with variations over the antenna array.

A great potential for lower correlation and utilization of less complex linear precoders was displayed in measurements [18]. This was achieved using large cylindrical antenna array used in the receiver. It was shown that with an increasing number of transmit antennas average channel correlation decreases. Also using linear pre-coding scheme 98% of dirty paper coding capacity can be reached only with 20 service antennas at the base station.

A configured 64 element antenna array is used for measurements [19] with different antenna array geometries like vertical and horizontal, planar. It was con-

cluded that the best antenna geometry for massive MIMO is horizontal. Whereas, use of vertical antenna geometry showed the worst results. Horizontal geometry gives the lowest average correlation coefficient with possibility to use even bigger number of antennas.

Another measurement performed in [20] is aimed to validate several theoretical channel properties for large scale antenna systems. Channel is measured creating virtual antenna array from single antennas moved one a rail by stepping motor. With an increasing number of elements in base station antenna array user channel orthogonality also increases. The whole multiuser channel gets hardened — small scale or fast fading is reduced. Due to a large antenna array a non-stationary phenomenon was observed at some locations of the measurement area.

A greater insight in delay spread properties is paid in [7] where 128 base station antennas and 38 mobile users with single antennas were used. When channel delay spread is comparable size or greater than the symbol duration an inter symbol interference problem may arise. This leads to poor reception and requires an equalizer at the receiver. Zero forcing may mitigate inter symbol interference and interference between users for conventional MIMO. However, that requires transmit power increase and noise enhancement. It was shown that these problems may be avoided in massive MIMO.

Limitation in degree of freedom is a problem induced by small number of antennas in wireless system. In massive MIMO, DoF has an important role and it is crucial to exploit all possible DoF up to the limit of number of antennas used. 64 antennas grouped into sets of 8 antennas are used in measurements [21]. Antenna sets are rearranged in 3 different geometrical forms — a square with antennas separated by the half wavelength distance at 5.8 GHz band, line of 2 meters and line of 6 meters with antennas spread along them. In these measurements it was observed that an increase in the number of antennas increases the DoF number and enhances system performance overall. Very large linear array shows the best results among other geometrical forms of antenna distribution in LOS and NLOS cases. It was also observed that channel characteristics such as received power or angle-of-arrival become non-stationary over the antenna array. This phenomena impacts the performance of the wireless systems. Therefore, it has to be attended in channel model of massive MIMO systems.

Measurements [5] with 128 antenna elements at 2.6 GHz frequency range are performed in order to study the key propagation characteristics required for massive MIMO channel model implementation. COST 2100 channel model is used as a base and new properties of massive MIMO channels that are missing in COST 2100 are identified. First insight is that a large scale/shadowing can be observed over the very large array, which can be critical for performance evaluation and design of algorithms for massive MIMO. Therefore, non WSS channel characteristics should be considered when implementing channel models for massive MIMO. A visibility region concept should be used at the base station side to evaluate spatial variations over the large array. A total number of visible clusters over large antenna array have to be determined since more clusters are visible for large arrays than to small arrays. A cluster visibility gain at base station side, which describes cluster power variations should be also modeled [5].

Chapter 3

Propagation Measurements

Measurement campaigns are essential part of wireless communication system implementation process. Insights of theoretical studies can be confirmed or denied and supplemented by real-life system implementations. Number of parameters can be investigated by studying the propagation channel behavior, parametrization and validation of channel models can be performed, etc. The few measurement campaigns discussed in previous chapter are aimed to study certain propagation characteristics and properties. However, more measurement campaigns should be performed for broad massive MIMO system investigation. We conducted one more channel measurement campaign which contributes to the all study with its findings.

The channel measurements were performed in a semi-urban area — Faculty of Engineering (LTH) campus, Lund University, Lund, Sweden. The measurement setup consists of the base station with a virtual very large array of about 7.5 meter length, which is positioned on the roof of a three story building facing four story buildings, as shown in Figure 3.1. Single antenna is moved by a stepper motor along the array with a distance of half of the wavelength. At the mobile station a single antenna was used. Measurements were performed for four MS positions where two of them were in non-line-of-sight and two in line-of-sight as indicated in Figure 3.1. In NLOS cases, MS is placed in positions MS1 and MS2 — at the north side of the parking lot in environment full of obstacles (trees, bushes, buildings, light poles). In LOS case MS is placed in positions MS3 and MS4 — at the south side of the parking lot where the MS is visible to the BS.

In order to study impact of: 1) operating frequency, 2) antenna polarization and 3) antenna directivity on channel response using very large array, measurements were performed using two center frequencies and different antennas with different polarizations. Measurements with the directive patch antennas at transmitter (Figure 3.2) and receiver (Figure 3.3) were carried out using 2.6 GHz and 5.1 GHz frequency bands, with VV and HH polarizations. For directivity studies two different antenna setups were used at 2.6 GHz. First time omni-directional antenna was used at the transmitter and directional patch antenna at the receiver side. Second time omni-directional antenna was used at both transmitter and receiver side.

Figure 3.1: Aerial photo of measurement area with BS and MS positions.

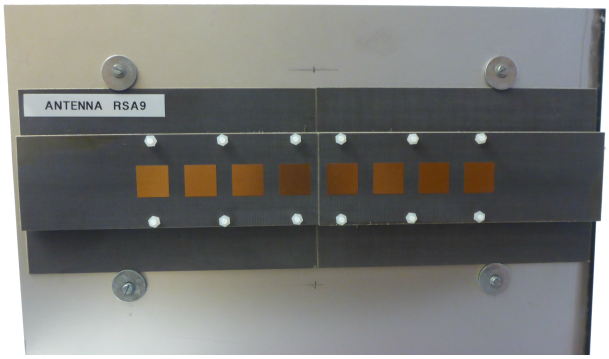

Figure 3.2: Transmitter antenna array. One antenna was used for transmitting while the rest of antennas were terminated.

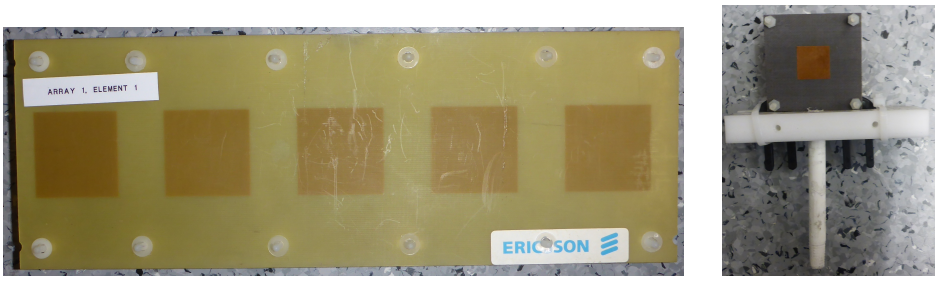

(a) **(b)**

Figure 3.3: Receiver antennas — a) for 5.1 GHz frequency, b) for 2.6 GHz frequency. In antenna array at a) one antenna was used for receiving the signal while other antenna ports were terminated.

During each measurement session a single antenna at BS is moving from east to west side along the rail to 128 and 256 equally separated positions when using 2.6 GHz and 5.1 GHz frequencies, respectively, while receiving signal from MS at each position in the rail. It takes about 10 minutes for the single antenna to travel throughout the array using 2.6 GHz frequency and about 20 minutes using 5.1 GHz frequency. In order to keep channel as static as possible channel measurements are performed at night when there are no moving objects. Summary of main measurement parameters is listed in Table 3.1.

Freq. band	Bandwidth	No. of array elements
2.6 GHz	40 MHz	128
5.1 GHz	200 MHz	256
5.1 GHz	40 MHz	128

Table 3.1: Differences between the measurement setups at 2.6 GHz and 5.1 GHz.

The equipment used for the measurement contains vector network analyzer (VNA), RF-to-optical/optical-to-RF converters, power amplifier, 200 meter fiber optic cable and a laptop computer. Setup scheme for this measurement campaign is depicted in Figure 3.4.

Rohde & Schwarz (ZVC, 20 kHz to 8 GHz) Vector Network Analyzer (Figure 3.5) generates the signal and measures the response of a network as a function of frequency of an applied RF signal. VNA can make hundreds of measurements per second rapidly measuring at one frequency at a time over user preset frequency bandwidth.

The RF signal from the VNA is fed into the RF-to-Optical converter (Figure 3.6), where it is converted into an optical signal. The signal travels via a fiber optic cable into Optical-to-RF converter (Figure 3.7) at the transmitting side of the system. Here, optical signal is converted back into the RF signal and it is fed into power amplifier. The fiber optic cable is used for lower attenuation since using copper cables usually results in a considerably high attenuation especially

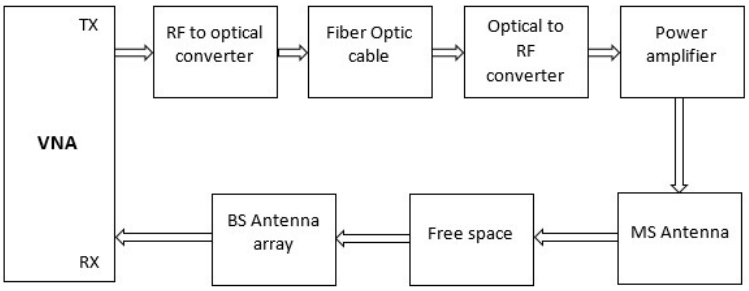

Figure 3.4: Measurement campaign equipment setup.

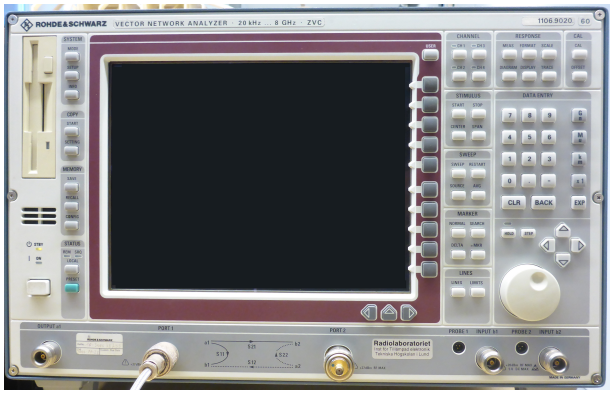

Figure 3.5: Rohde & Schwarz ZVC vector network analyzer used for the measurements.

in longer distances.

Figure 3.6: Optical Zonu OZ9000 RF-to-Optical converter.

However, in order to overcome significant path loss during the transmission over the air interface, signal from the optical to RF converter is fed to amplifier which enhances power level of the RF signal. Therefore, the signal transmitted from antenna have high enough power to achieve required signal to noise ratio at the receiver. Amplifier outputs 1 W (30dBm) signal to transmitting antenna.

In total 24 measurement sessions were performed — 16 sessions for four positions, two frequencies and two polarizations, 8 sessions for four positions, one frequency and two different antennas. Raw data collected from the measurements contains transfer function of the single-input multiple-output (SIMO) channel which is used for getting impulse response estimates (IRES) illustrated in Figure 3.8. Each transfer function has 1601 frequency points covering 40 MHz

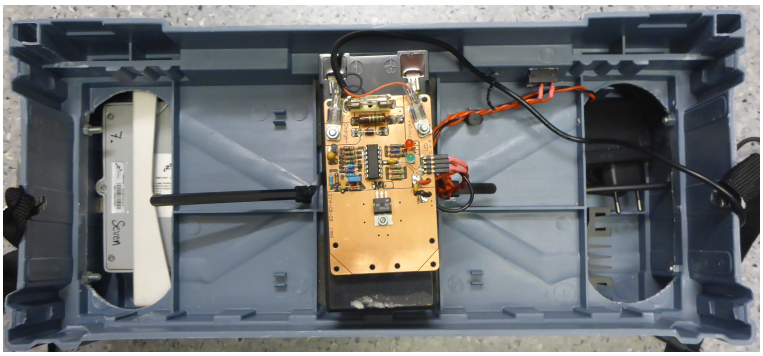

Figure 3.7: Optical-to-RF converter.

bandwidth at 2.6 GHz frequency and 200 MHz bandwidth at 5.1 GHz frequency. A sliding window is applied for MPC extraction selecting a subset of antenna elements each time. The width of the window is about 0.57 m and it contains 10 and 20 adjacent antenna elements over the array at 2.6 GHz and 5.1 GHz bands, respectively. An example for 2.6 GHz band is illustrated in Figure 3.9. When using an antenna window, the channel can be considered as wide-sense stationary which enables spatial-variation study of the channel over the antenna array. Also, when SAGE (Space-Alternating Generalized Expectation-Maximization) algorithm is applied for directional estimation using the moving antenna element window gives considerably high angular resolution [5]. The moving antenna takes 119 positions where it is shifted by 1 and 2 antenna elements at the 2.6 GHz, and 5.1 GHz frequency bands, respectively. SAGE algorithm is applied to the IRES at each window position in order to extract delay, angle-of-arrival and complex amplitude of each MPC, where 10 MPCs are extracted at each delay above the noise floor.

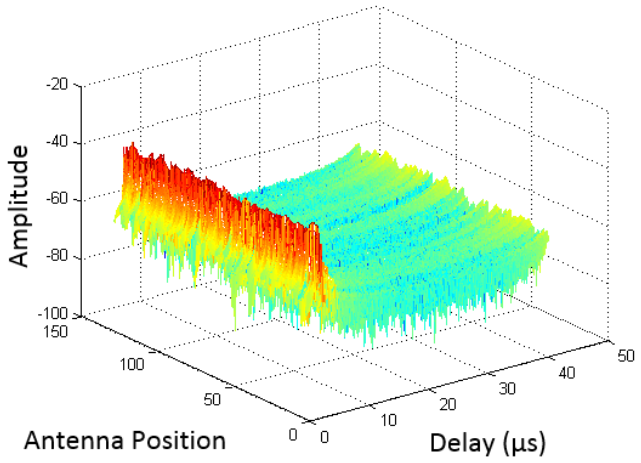

(a)

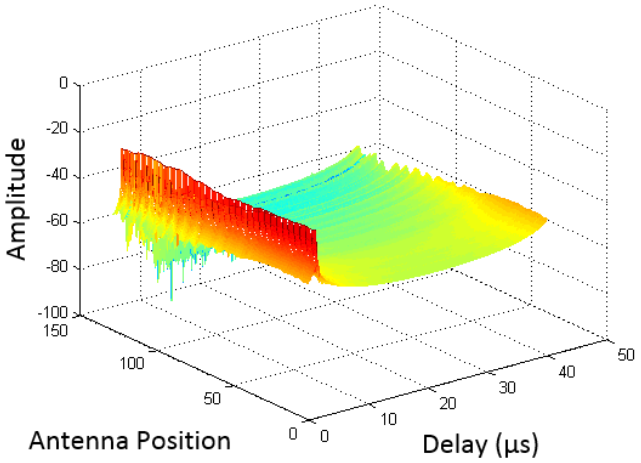

(b)

Figure 3.8: Estimated Impulse Responses for 2.6 GHz band in (a) NLOS conditions and (b) LOS conditions.

Figure 3.9: Sliding antenna window for 2.6 GHz band containing 10 adjacent antennas.

Chapter 4

Propagation channel parameter estimation

As it was already mentioned, multiple antennas used at the transmitter and receiver increase the capacity of mobile radio communication systems and overall performance of the system. However, in order to design and implement such systems realistic radio channel models have to be employed. These channel models have to be experimentally validated in order to ensure that they are able to capture essential characteristics of radio channels, which can affect the performance of investigated wireless communication system. Efficient and sophisticated computational method has to be applied in order to extract these essential characteristics. There is a number of high resolution approaches for channel parameter estimation, which can be categorized in three groups — spectral estimation (Multiple Signal Classification (MUSIC) algorithm), parametric subspace-based estimation (Estimation of Signal Parameter via Rotational Invariance Techniques (ESPRIT) algorithm), and deterministic parameter estimation (Expectation maximization (EM) algorithm). Among others in third group there is also Space-Alternating Generalized Expectation-Maximization (SAGE) algorithm. EM algorithm is a two-step iterative method for a maximum-likelihood approximation. At the first step of the EM algorithm, which is referred to as expectation step, log-likelihood function is calculated. At the second step, which is referred to as a maximization step, calculated parameters are updated by maximizing the function from expectation step. EM algorithm simultaneously updates all parameters for channel estimation and the detection of data, which results in slow convergence. Whereas, SAGE algorithm can accelerate the convergence of EM algorithm by updating parameters sequentially. In this work SAGE algorithm is used for channel parameter estimation [22].

4.1 SAGE algorithm

SAGE algorithm is a high resolution algorithm used for joint parameter of given superimposed signals estimation. From the received signal SAGE algorithm can estimate such parameters of multipath components as delay, AoA and complex power. These results can be used for identifying physical scatterers and determining cluster visibility over the array [23].

SAGE algorithm consists of two main steps — initialization and iteration step. In the initialization step the entries of parameter vector θ_l characterizing the

impinging wave l are estimated. This parameter vector $\theta_l = [\Omega_{1,l}, \Omega_{2,l}, \tau_l, \upsilon_l, \alpha_l]$ consists of five parameters. Angle-of-departure, $\Omega_{1,l}$, and angle-of-arrival, $\Omega_{2,l}$, parameters denote in which direction wave is propagated and from which direction impinging wave arrives. Propagation delay, τ_l, defines the amount of time signal travels from transmitter to receiver. Doppler frequency, υ_l, indicates the shift of frequency due to movement of receiver. Complex weight, α_l, defines received complex signal power. At first parameters of the dominant paths are estimated. Then initialization step employs successive interference cancellation method (SIC) where an estimated interference of previously estimated waves is subtracted from the received signal [23]:

$$y^l(t) = y(t) - \sum_{l'=1}^{l-1} s(t; \hat{\theta}_{l'}(0)) \tag{4.1}$$

Iteration step of SAGE algorithm re-estimates the parameter vector θ_l of the impinging wave l. In SAGE algorithm iteration cycle consists of M number of iteration steps where parameter vector is re-estimated for each wave. Iteration cycle runs until it reaches convergence, the point when there is no significant update of parameter vector entries [23]. In this work, SAGE algorithm is used to extract angle-of-arrival in azimuth angles, propagation delay and complex weight for each MPC. Doppler frequency, angle-of-departure (AoD), elevation angles are not estimated as MS is not moving during the measurements and only one antenna is used at MS.

4.2 Multipath clusters

Radio wave propagation measurement results show that multipath components do not arrive at the receiving point uniformly in delay-angular space. Usually due to propagation effects as scattering, diffraction, reflection caused by the environment, transmitted energy is concentrated in clusters. Each cluster is defined as a set of MPCs that contain similar delay-angular parameters — azimuth angle-of-arrival, azimuth angle-of-departure, elevation angle-of-arrival, elevation angle-of-departure and propagation delay — as well as powers over time. Similarity of delay-angular parameters in a cluster is normally caused by MPCs interaction with the same object in the environment. Based on this, clusters are considered to represent different groups of scatterers in a propagation channel [8].

Cluster-based channel models have more advantages over other channel models due to their ability to address channel variations in time and space. This is achieved by considering cluster characteristics like a visibility region concept, a non-stationary phenomena, delay and angle spread [5].

4.3 Multipath cluster identification

Originally visual inspection is performed in order to accurately identify multipath clusters. However, for the radio propagation measurements with large amounts of data, clustering based on visual inspection consumes too much time.

Therefore, automatic clustering algorithms are introduced, which group MPCs into clusters according to their delay-angular parameters. These automatic clustering algorithms can be categorized in two main groups — joint delay-angular clustering and sequential delay-angular clustering [28].

Joint delay-angular clustering uses total distance measure, which defines how similar the values of particular MPCs are jointly in both domains — angular and delay. Sequential delay-angular clustering is more attractive than joint delay-angular clustering because clustering in such algorithms is performed separately in both domains. At first clustering is performed in the delay domain and then based on the identified cluster delays', clustering is done in the angular domain. This approach solves the multidimensional problem as there is no need for one universal normalized value for both measured dimensions [28].

After defining initial expected number of clusters, automatic clustering algorithms assign all extracted MPCs to their clusters based on their parameters and eventually estimate the total number of clusters in the propagation environment. Most commonly used automatic clustering algorithms are K-Power Means, which clusters channel parameters taking into consideration the power of MPCs, fuzzy-c-means algorithm, which is similar to K-power means, and Multi-reference detection of Maximum Separation (MR-DMS) [28].

K-Means algorithm requires defining initial maximum possible number of clusters in the propagation channel being examined. When the number of clusters is set, the initial positions of the clusters centroids have to be calculated. Centroid of the cluster is defined as the center of the cluster and it is found by calculating power weight average in each dimension of MPC parameters. MPCs are then assigned to the nearest clusters based on the distance — difference of parameter values — from the clusters' centroids. After that new positions of clusters' centroids have to be calculated. MPCs are assigned to the closest centroids and centroid positions are recalculated until there is no significant movement of clusters' centroids anymore. A measure for distance between MPC and centroid is required when assigning MPCs to the clusters' centroids. Here, the multipath component distance (MCD) was introduced, which normalizes and scales different dimension data — time and angles of arrival. MCD is calculated as the Euclidean norm of vector containing normalized distances in delay and angular domains. Since at the beginning the initial maximum possible number of clusters is not known, the K-Means algorithm has to be run several times using different number of possible clusters. The most optimal number is then set by a Cluster Validity Index (CVI) which numerically measures the cluster separation and compact level of grouping MPCs [29].

Fuzzy-c-means clustering is similar to K-Power Means algorithm. However, a soft decision of MPCs' dependence to centroids is provided and a degree of membership is added to distance calculations. At first an initial number of clusters and their centroids have to be indicated. Then a distance with degree of membership between MPCs and their centroids is calculated. MPCs are reassigned to the new closest centroids based on distance calculations. New positions of centroids are then calculated. If the maximum number of algorithm iterations is reached then the algorithm is terminated at this point. If the new positions of centroids do not differ significantly from previously calculated positions then the algorithm is

terminated. If the positions of centroids change then the algorithm has to be repeated from the beginning. Results of fuzzy-c-means algorithms are evaluated by one of the CVIs — validity measure of separation and compact level [29].

Multi-reference detection of Maximum Separation (MR-DMS) is an algorithm based on the hierarchical clustering. At the beginning only one cluster is considered which is divided in two smaller clusters. New clusters are again divided in two smaller clusters and cluster division is performed until the predefined maximum number of clusters is reached. A cluster is divided into two clusters based on the maximum distance change among MPCs and reference point in single cluster. So the distances between each MPC and a reference points are calculated and then stored in ascending manner for each cluster. This approach for clustering has considerably low complexity and no knowledge of initial maximum number of clusters is needed. However, a considered number of well distributed reference points is required for this algorithm in order to be accurate enough. An adjustment of number of reference points and their distribution brings the complexity into the algorithm. MR-DMS also requires a careful selection of the CVIs as in the K-Means algorithm [29].

Automatic clustering techniques help to identify clusters in a fast and efficient way. However, they might be not accurate enough. In order to use any automatic clustering algorithm an initial number of existing clusters in examined propagation environment is usually required. The number of clusters can be named easily when the synthetic data is used for analysis. However, actual number of clusters cannot be named for experimental data. So the automatic clustering algorithm becomes more complicated and has to be run several times for determining the optimal number of clusters. A number of CVI techniques are created for numerically evaluating and selecting the optimal number of clusters. However, they are not able to always predict the correct number of clusters. Finally, for large pools of experimental data there is also a probability of merging two adjacent clusters or creating too many of them [29].

Visual clustering can bring more reliable and much simpler identification of MPC clusters when the data pool is not that large. Considerably accurate cluster identification can be performed especially when only one or two multipath parameter domains are taken into consideration. In this thesis work sequential-based visual inspection clustering method is used. With only 4 MS positions data pool is not large for visual inspection. Since the propagation environment is known identified clusters of MPCs can be related to the IOs in the environment.

4.4 Cluster identification approach

Based on the fact that the measurement environment is well known in this measurement campaign, extracted MPCs are grouped into clusters using visual investigation method. Sequential delay-angular clustering method is applied in this work. Therefore, at first clusters are identified in delay domain from power delay profiles (PDPs) at each MS position. Delay windows represent the MPCs arriving at the receiver with the same or similar propagation time. Based on identified clusters in delay domain, MPCs are then clustered considering their

AoAs and power distribution over the array. By knowing the position of the moving antenna window, directional and delay information, identified clusters can be related to IOs in propagation environment.

For example, for NLOS case when MS is in position 1 at 2.6 GHz band, significant MPCs arrive to the receiver in two delay bins. First peak above noise floor in the PDP represents first group of MPCs with considerably high power that arrive starting at around 1.48 μs delay to the receiver and that is considered as first delay-window. Second peak in the PDP indicates another group of MPCs with significant power that arrive to the receiver starting at 1.95 μs delay and that is considered as second delay-window. Conditioned on delays of identified delay-windows, MPCs are grouped into clusters based on their AoA depicted in Figure 4.1a and Figure 4.1c, and power distribution over the array depicted in Figure 4.1b and Figure 4.1d. It is visible in the figures how the described parameters change as the function of the moving antenna window. In first delay-window, we can see clusters of various sizes and most of them are visible only for a short part of the array. There is no single direction of arrival observed but rather scattered distribution. Clusters in this delay-window can be considered as reflections from the walls of the building in front and on the left side of the array and other physical objects in the environment which can be seen in Figure 4.3. Second delay-window contains group of MPCs that arrive at the receiver mostly at around the same angle (80 degree). However, there is a significant decrease of power following a change of the angle-of-arrival for some positions at the end of the array, thus two clusters are identified in this delay-window. Here, both clusters are considered as a reflection from the part of building in front of the array (Figure 4.3). Therefore, reflected signal is received at all antenna window positions except at the noted fade close the end of the array. Different behavior is observed in LOS case when MS is in positions 3 at same 2.6 GHz band. All the significant MPCs arrive at the receiver in one delay-window starting at around 1.28 μs. Conditioned on the identified delay-window, MPCs are grouped into one cluster based on their AoAs visible in Figure 4.2a and power distribution over the array in Figure 4.2b. Most of the MPCs arrive at around the same angle-of-arrival (between 30 and 40 degree) with the most of the power concentrated at the beginning of the array. This cluster is considered as LOS component which is visible at all array positions.

Rather similar results as in 2.6 GHz band are received at 5.1 GHz band in both NLOS (Figure 4.5) and LOS (Figure 4.6) cases when MS is in the same position 1 but with a bit higher resolution. In NLOS case there are two delay-windows starting at 1.5 μs and 1.99 μs. As can be seen in Figure 4.5a at first delay-window, groups of MPCs arrive at around 40 degree, 60-80 degree and 120-140 degree angles which are similar at 2.6 GHz band. However, in this case distribution of AoAs is more consistent and clusters are visible for longer parts of the array. Identified clusters are considered as reflections from the walls of the building close to the array (Figure 4.4). At the second delay-window, there is a group of MPCs that arrive at around 80 degree (Figure 4.5c) which is the same as the 2.6 GHz band and thus, clusters are related to same IOs (Figure 4.4). Same tendency is followed in LOS case where results at 5.1 GHz band are similar to results at 2.6 GHz band but with a higher resolution. This can be seen in Figure 4.6. All significant MPCs arrive at one delay-window starting at around 1.31 μs. Only one main cluster is

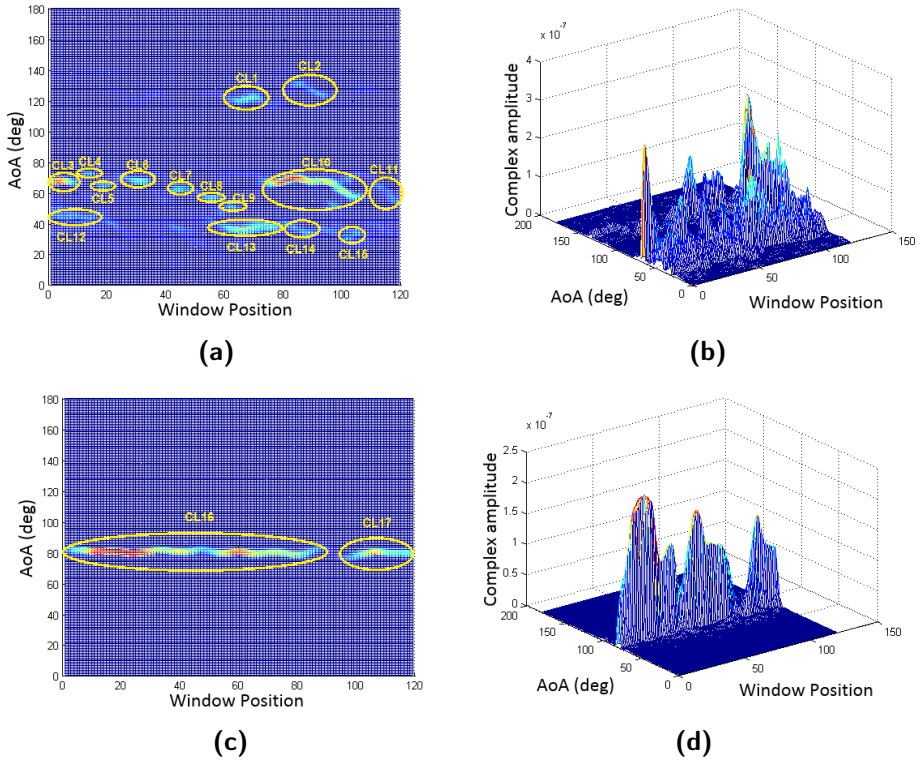

Figure 4.1: Power distribution of MPCs of the clusters over AoA and over the array for NLOS condition (MS in position 1) at 2.6 GHz band. (a) and (b): first delay window; (c) and (d) second delay window.

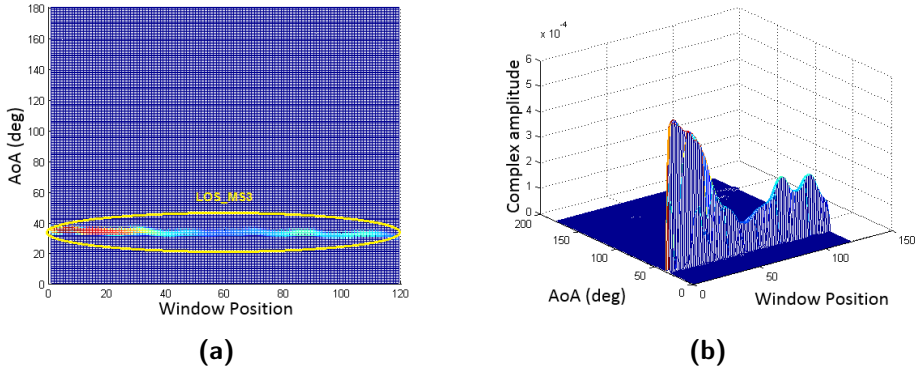

Figure 4.2: Power distribution of MPCs of the clusters over AoA and over the array for LOS condition (MS in position 3) at 2.6 GHz band.

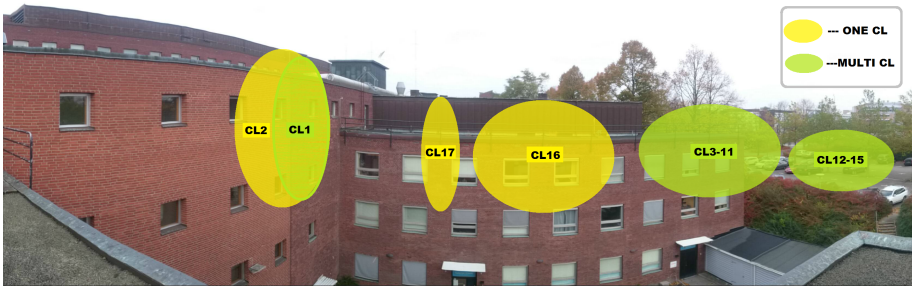

Figure 4.3: IOs in the environment that are associated with the identified clusters of Figure 4.1 (a) and (c).

Figure 4.4: IOs in the environment that are associated with the identified clusters of Figure 4.5 (a) and (c).

visible in Figure 4.6a which can be considered as LOS component and it is around 40 degree angle-of-arrival. There is also a small number of weak MPCs arriving at around 150 degree angle. These MPCs are considered as reflections from the wall on the left side of the array and they contribute with most of the power at the last antenna window positions which are closest to the wall (Figure 4.7).

There is a slight change in results when omni-directional antenna is used at the receiver and transmitter in NLOS. MPCs arrive at the receiver in three delay-windows. At first delay-window, MPCs arrive with 0.75 ns delay and their AoAs together with the power distribution can be seen in Figure 4.8a and Figure 4.8b. Clusters here are of similar sizes and they are visible for short parts of the array at the angles of 0–20 degrees and 160–180 degrees. At second delay-window MPCs, arrive starting at around 1.48 μs delay and their AoAs are varying (Figure 4.8c and Figure 4.8d) in a similar manner as in previously discussed cases with 2.6 GHz and 5.1 GHz bands. There is also a considerably consistent cluster of MPCs at around 80 degree angle-of-arrival which is also observed when using other antennas. It is considered as the reflection from the wall of the building in front of the array. Other MPCs are arriving between 20 and 40 degree angles. At the third delay-window MPCs, arrive starting at around 2.45 μs delay between angles of 10–30 degrees and 140–170 degrees (Figure 4.8e and Figure 4.8f). These are MPCs contributed by the wall on the left side of the array and by other objects in propagation environment.

In LOS case significant MPCs are received at around 40 degree angle starting

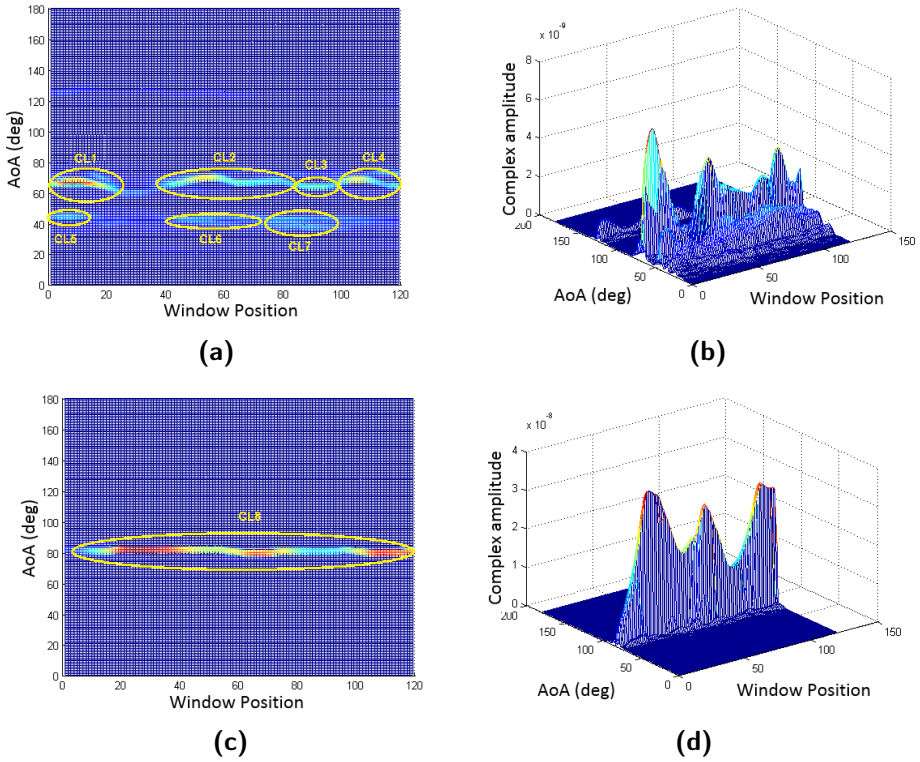

Figure 4.5: Power distribution of MPCs of the clusters over AoA and over the array for NLOS condition (MS in position 1) at 5.1 GHz band. (a) and (b): first delay window; (c) and (d) second delay window.

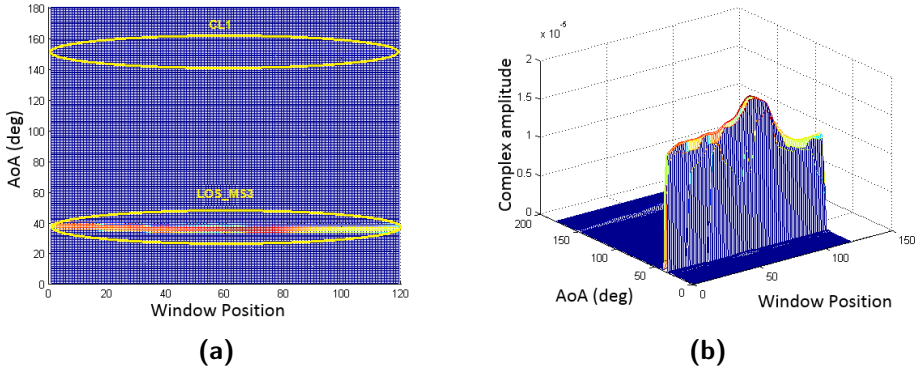

Figure 4.6: Power distribution of MPCs of the clusters over AoA and over the array for LOS condition (MS in position 3) at 5.1 GHz band.

Figure 4.7: IOs in the environment that are associated with the identified clusters of Figure 4.6 (a).

at around 1.28 μs delay (Figure 4.9). MPCs carrying most of the power are observed at the beginning of the array and with attenuation over the rest part of array. There is also a contribution at around 150-160 degrees angles which is reflection from the wall on the left side of the array. When using omni-directional antenna in LOS distribution of AoAs of MPCs are close to those of previously discussed cases with directive antennas and 2.6 GHz and 5.1 GHz bands. However, distribution of AoAs is not that consistent in this case and observed clusters are visible for short parts of the array.

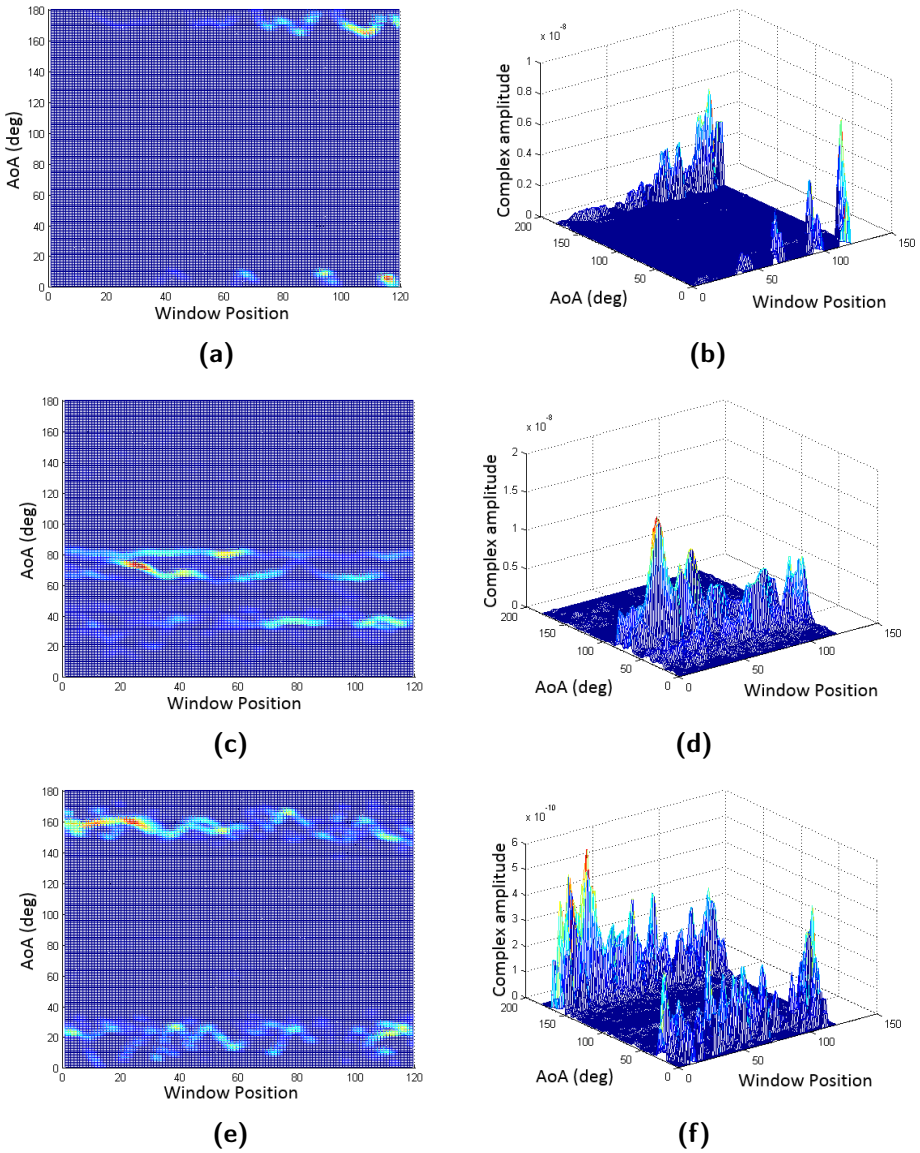

Figure 4.8: Power distribution of MPCs of the clusters over AoA and over the array for NLOS condition (MS in position 1) at 2.6 GHz band with omni-directional antenna. (a) and (b): first delay window; (c) and (d) second delay window, (e) and (f) third delay window.

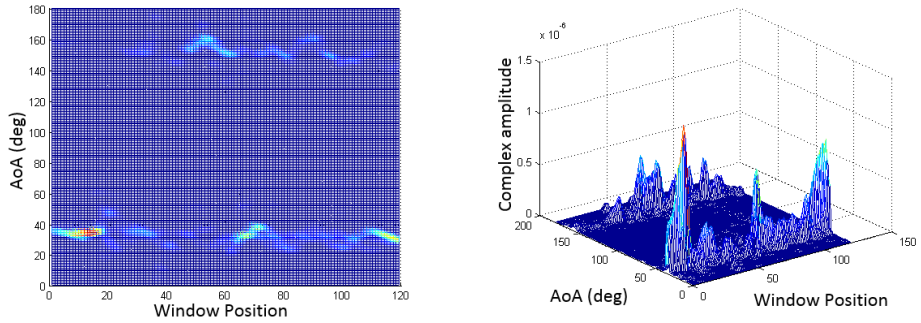

(a) **(b)**

Figure 4.9: Power distribution of MPCs of the clusters over AoA and over the array for LOS condition (MS in position 3) at 2.6 GHz band with omni-directional antenna.

4.5 Cluster parameters

Previous sections introduced different methods for cluster identification and cluster identification approach in this thesis work. This section presents the cluster parameters that are extracted for identified clusters in this thesis work. At first, cluster visibility regions are defined followed by introduction to cluster delay and angle spread. Cluster power decay and shadow fading factor are then described. The section concludes with the discussion on correlation among cluster parameters.

4.5.1 Cluster visibility regions

Visibility regions (VR) are defined when modeling clusters of scatterers. In COST 2100 channel model cluster visibility region is defined as a circular region on the azimuth plane in the area which determines the visibility of cluster — cluster is active in that area. Each cluster has at least one visibility region. Cluster becomes "visible" to MS when MS enters clusters VR, then their MPCs contribute to the channel between the MS and the BS. The power variation of the scattering contribution in each VR is described by a visibility gain function. Power level can be controlled then in each VR with the help of this function. When MS is moving it can enter and leave the VRs of different clusters. There is also a possibility of MS appearing in the area where several VRs overlap. Therefore, several clusters are visible simultaneously to the same MS [5]. Since channel time and space variations are caused by the movement of MS, some channel models use cluster VRs only at the MS side. However, due to the large antenna arrays the effect of spatially variant channel can be observed in massive MIMO base stations as well, which leads to that each cluster should have two VRs — one VR at the mobile station (MS-VR) and one VR at the base station (BS-VR). Because of the movements of mobile station, cluster can be seen when MS is inside MS-VR. When the large antenna array is used some antennas at the base station can be inside BS-VR and some of them outside BS-VR as depicted in Figure 4.10. Properties for MS-VR

and BS-VR such as size and shape have to be described for the channel model separately. This is required because the propagation environment from MS and BS to the cluster is different — MS are usually on the ground whereas BS is normally located on the buildings [5].

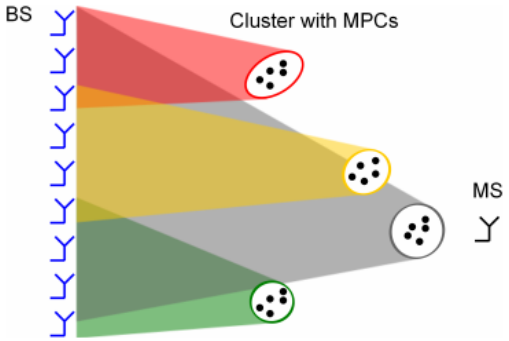

Figure 4.10: Base station visibility regions of clusters [5].

Because of the large size of antenna array in massive MIMO systems each array element may observe different group of clusters. Therefore, each array element receives signals which experienced different propagation channel. Some groups of clusters or a single cluster may be observable for more than one antenna if they are less separated. In that case antennas share that cluster or the cluster group. An appearance and disappearance of clusters in large sized arrays is characterized by birth death process. A group of visible clusters is determined for each antenna on time and array. Parameters for each cluster are determined by updating geometrical relationships considering the cluster and receiver movements. It has to be noted that parameters differ for newly observable clusters and "survived" clusters. Delay spread on each antenna becomes different for the whole array. Eventually, the wide-sense stationary assumption is not valid for large scale antenna array as it is for conventional MIMO systems [24].

4.5.2 Delay spread

Due to complex environments a propagation channel constitutes of several multipaths — transmitted signals undergo diffraction, reflection or scattering that cause signal strength attenuation, shift of frequencies, change of phase, and delays. After interaction with objects in propagation environment a number of delayed replicas of the original signal may arrive to the receiver through different paths. IOs with very smooth surfaces may be modeled as specular reflectors where only one MPC is in the cluster. IOs can also be modeled as a cluster of a number of MPCs where each MPC is associated with set of parameters such as complex amplitude, angle-of-arrival and delay. MPCs' parameters in one cluster are closely related in both time and angular space. However, propagation time of the first and last arriving significant MPC within a cluster differs. Delay spread inside each cluster and existence of clusters with different delay centroids may cause inter symbol

interference (ISI) which limits the symbol rate in multipath propagation. Delay dispersion parameters for each cluster are defined starting with time-integrated power computation [8]:

$$P_m = \int_{-\infty}^{\infty} P_h(\tau) d\tau \tag{4.2}$$

Mean delay is given by:

$$T_m = \frac{\int_{-\infty}^{\infty} P_h(\tau)\tau d\tau}{P_m} \tag{4.3}$$

And finally rms delay spread is given by:

$$S_\tau = \sqrt{\frac{\int_{-\infty}^{\infty} P_h(\tau)\tau d\tau}{P_m} - T_m^2} \tag{4.4}$$

Where τ is propagation delay, $P_h(\tau)$ is power at the delay.

4.5.3 Angle spread

Angle-of-arrival is one of the characteristics describing MPCs arriving at a wireless receiver. Due to different propagation mechanisms caused by IOs in the propagation environment multipath power spread can be observed in azimuthal directions. Angular spread is a relevant propagation parameter as it provides information about multipath power spread or concentration in the horizon. Angle spread can be found by:

$$\sigma_\theta = \sqrt{\frac{\int_{-\pi}^{\pi} (\theta - \overline{\theta})^2 p(\theta) d\theta}{\int_{-\pi}^{\pi} p(\theta) d\theta}} \tag{4.5}$$

Where θ is angle-of-arrival, $\overline{\theta}$ is centroid of azimuth spectrum, p(θ) is power at the angle [24] for each cluster of MPCs.

Angle spread describes scattering radius of the cluster. Cluster angle spread may be estimated for azimuth and elevation for both transmitter and receiver. However, in this thesis work only angle spread at the receiver in azimuth directions is estimated.

4.5.4 Cluster Power Decay

In general it is considered that average cluster power is exponentially decaying with the delay of the cluster [30]. However, variation of cluster power contribution can also be observed over the large antenna arrays. When there is a large number of antenna elements, different antennas may receive distinct amount of power from the observed cluster. Power decay of the cluster over the array is characterized by the slope of its linear regression line.

4.5.5 Cluster Shadow Fading Factor

As mentioned in subsection 4.5.1 due to the size of large antenna arrays a cluster may be observed by several antennas and thus, cluster visibility region at the BS side is introduced. Clusters spanning over several array elements might undergo shadow fading which is defined as attenuation in received signal power due to multiple random factors (i.e. shadow caused by high-rise building, random IOs between transmitter and receiver). Cluster power deviation from the linear regression line is defined as cluster shadow fading. Here cluster shadow fading factor is defined as standard deviation, σ_{Shf}, of shadow fading [31].

4.5.6 Cluster parameter interdependence

As mentioned before, clusters are defined as a group of MPCs showing similar or same parameters — usually angles of arrival, delay and complex power. These parameters might correlate in each cluster which has to be addressed in channel models to be physically relevant. Investigating correlation of parameters helps to identify and analyze clusters. By employing two concepts — correlation coefficient and multidimensional kernel density estimate — the cross-correlation of cluster parameters was investigated in [27]. No or low, strong negative correlations among parameters can be observed. Strong correlation is identified between power of the cluster and the number of MPCs in it. The more MPCs there are within a cluster, the more power it contains. There is possibility of high power even if the number of MPCs is not big. This might occur when MPCs are coming from dominant scatterers carrying strong power and having small spread [27]. It is known from radio wave propagation that early arriving waves carry more power than the ones arriving after longer delay. The correlation between power and mean delay exists. There is also strong correlation observed between delay spread and angular spread which describe the size of the cluster. When large angular spread is observed at transmitter side, it is also seen large at the receiver side — delay spread in this case is also observed to be large [27]. AoA cluster azimuth spread defining the size of the cluster has a strong correlation with a number of clusters. When there is a big number of clusters usually they are of a small azimuth AoA spread [27]. In this thesis work correlations between delay spread and angle spread, delay spread and shadowing, angle spread and shadowing, within each cluster are studied. These three parameters of interest, angle spread, delay spread, and shadowing, are extracted from measurements with large antenna array at the BS side. Cluster parameters are estimated for each cluster as a function of moving 0.57 meter antenna window. Estimated parameters for one cluster over the antenna array are illustrated in Figure 4.11. Finally correlation of parameters within each cluster are estimated.

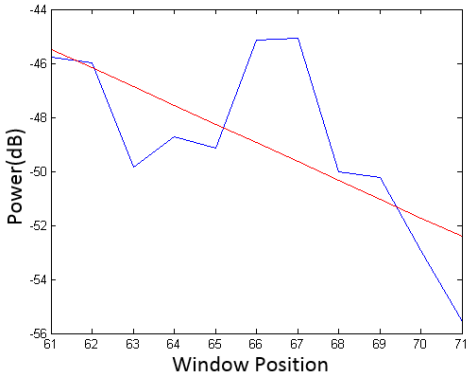

(a)

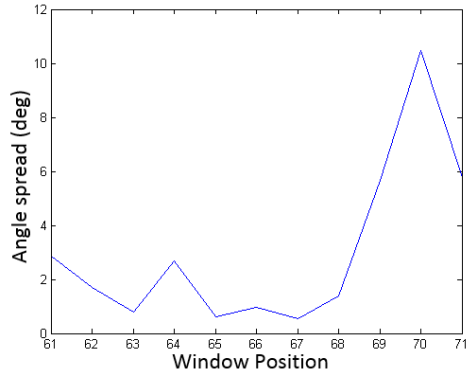

(b)

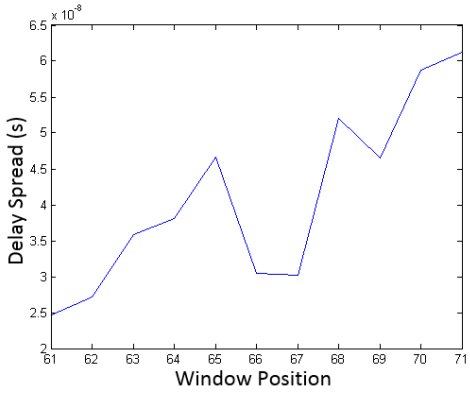

(c)

Figure 4.11: Estimated cluster parameters. (a) Power variation with linear regression line, (b) Delay spread and (c) Angle spread within cluster over the antenna array.

Chapter 5
Data analysis

The previous chapters covered the details about measurement setup and environment, extraction of multipath components for further processing, clustering and cluster parameter estimation. This chapter covers the analysis of collected data. Based on earlier described clustering approach identified clusters are analyzed and results of different setups are compared to report the observed effects of the frequency band, antenna polarization, and antenna directivity on the characteristics of the clusters.

5.1 Impact of frequency band, polarization and propagation condition

5.1.1 Number of clusters

As mentioned before, measurements at 2.6 GHz band and 5.1 GHz band were performed using different frequency bandwidths — 40 MHz and 200 MHz, respectively. Since we used sequential clustering method, clusters were identified in delay domain at first and then in angular domain. Despite the fact that different frequency bands were used, clustering results in the delay domain are very similar. It is found that both bandwidths are able to capture the significant contributions of IOs in the environment in the delay domain. When performing clustering in angular domain as it was discussed in previous chapter it was noticed that AoAs of MPCs are distributed in similar manner at both bands. Here we can see that the same IOs are identified in both cases. However, power variation in clusters is different at both bands. Therefore, when applying 20 dB threshold for NLOS and 30 dB threshold for LOS to eliminate weak clusters, the number of clusters, N_c, differs for both frequency bands in NLOS case. This also applies for the cases when different polarizations are used. Power variation in clusters using VV polarization rather differs from HH polarization and thus, after applying the threshold, numbers of clusters slightly alter. It is visible in rows 1 and 3 of Table 5.1 that when VV polarization is used, the number of clusters is higher than with HH polarization in NLOS case and same number of clusters is identified for both polarizations in LOS case. For frequency band comparison, number of clusters is slightly higher for 2.6 GHz band in NLOS case whereas in LOS case there is no difference. After applying the threshold, power contribution to the antenna array by remaining

clusters may vary accordingly to their observed BS-VR, number of MPCs per cluster, propagation condition. In NLOS condition the number of clusters is higher than in LOS condition. However, most of the clusters identified in NLOS contain small observed BS-VRs except the cluster spanning almost over the entire array. There is a difference in power contributions among the clusters observed in NLOS conditions. However, even bigger differences are visible between the strong and weak clusters in LOS conditions. That is confirmed in rows 2 and 4 of Table 5.1 where dynamic range values are presented. It is visible in the Table 5.1 that this ratio of strongest and weakest clusters has lower values for 5.1 GHz band than 2.6 GHz in NLOS and bigger values in LOS. Polarization at 2.6 GHz band has no significant effect on the ratio while it is somewhat different at 5.1 GHz band. Slightly higher dynamic range values are visible for HH polarization in both LOS and NLOS conditions for 5.1 GHz band.

Freq. band	2.6 GHz	2.6 GHz	5.1 GHz	5.1 GHz
Bandwidth	40 MHz	40 MHz	200 MHz	200 MHz
Polarization	VV	HH	VV	HH
NLOS				
N_c	36	34	30	25
Dynamic range (dB)	23.26	24.85	20.91	22.42
LOS				
N_c	7	7	7	7
Dynamic range (dB)	29.71	29.90	30.931	34.00

Table 5.1: Number of clusters and dynamic range for both frequency bands and polarization, in NLOS and LOS conditions.

5.1.2 Observed length and visibility gain of clusters

After cluster identification in each case, we observe that many clusters are not visible over the entire array. This can be seen in Figure 5.1 where number of clusters and their lengths are illustrated for NLOS and LOS conditions, respectively. In Figure 5.1a, we can see that in NLOS case, most of the clusters are between 1 and 3 meters length. With the increasing size of observed BS-VR, number of identified clusters decreases. Only one cluster which contains observed BS-VR that is around 7 meters is visible in NLOS case. There is no significant difference observed between results for different frequencies or polarizations. Just a slightly larger number of clusters is visible for 2.6 GHz band. There are also hardly more clusters when VV polarization used for some observed cluster lengths.

Rather different situation is observed in LOS case where a much smaller number of clusters is identified. We can see in Figure 5.1b that most of the observed clusters are around 1 to 4 meters length for both frequency bands. There is no significant difference visible among observed lengths between different polarizations. There are 2 clusters identified for each frequency band and polarization where their observed BS-VRs are around 7 meters length. This is more than in

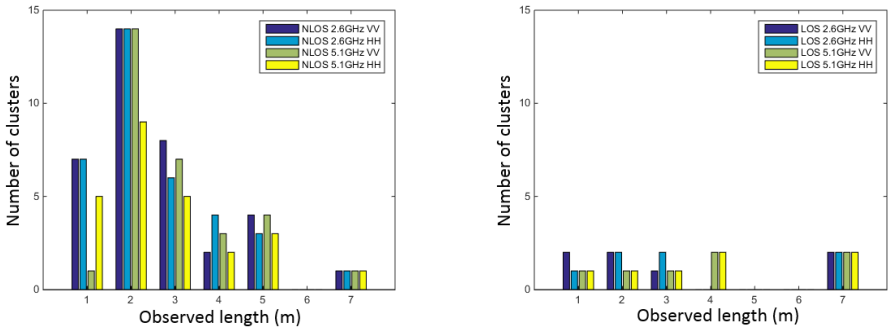

Figure 5.1: Observed length of clusters in meters for NLOS (a) conditions and LOS (b) conditions.

NLOS where only one cluster of such size is observed for each case. Here a LOS contribution is observed since MS is visible to antenna array. In addition to that there is also a considerably strong reflection from the wall on the left side of the array which contributes over the whole array. For some clusters that contribute over short part of the array or over the whole array, their power contributions vary significantly. Here it is considered that large-scale fading/shadowing can be experienced due to multipath interaction with IOs when using very large antenna array. Consequently, massive MIMO channel cannot be seen as a wide-sense stationary. In order to observe cluster power variation for each observed BS-VR a linear slope in dB is estimated. It is visible in Table 5.2 where the mean values of the slopes are presented that somewhat higher values are estimated for 2.6 GHz band than for 5.1 GHz in both NLOS and LOS cases. For 5.1 GHz band slope of cluster power variation is close to 0. Also higher power variations are visible when HH polarization is used. The difference can also be seen in cumulative distribution functions (CDFs) of slopes for each case in Figure 5.2.

Freq. band	2.6 GHz	2.6 GHz	5.1 GHz	5.1 GHz
Bandwidth	40 MHz	40 MHz	200 MHz	200 MHz
Polarization	VV	HH	VV	HH
NLOS				
Slope (dB/m)	-1.15	2.87	0.01	0.4
LOS				
Slope (dB/m)	-2.26	2.64	-0.08	-0.37

Table 5.2: Mean values of the slopes for both frequency bands and polarization, NLOS and LOS cases.

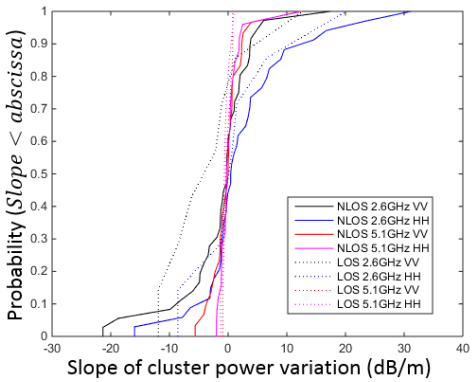

Figure 5.2: Slopes of cluster power variations for their BS-VRs for both frequency bands and polarizations, NLOS and LOS cases.

5.1.3 Delay spreads of clusters

One of the most important parameters giving statistical description of the multipath effects, delay spread, σ_τ, is calculated for each cluster using equations 4.2–4.4. Since the bandwidths used at both frequency bands differ, measurement data at 5.1 GHz band is reprocessed to 40 MHz bandwidth for the fair comparison of delay spreads. Reprocessing of data is done by selecting one fifth of the frequency bins in the middle of 200 MHz bandwidth. Then, having measurement data for 2.6 GHz and 5.1 GHz bands at 40 MHz bandwidth, CDFs of delay spreads for both bands are presented in Figure 5.3. There is a distinct difference in results for LOS and NLOS conditions. Clearly, lower values of delay spread are received when MS is in LOS. It is also observed that delay spread at 5.1 GHz is noticeably lower than at 2.6 GHz band. However, there is no clear impact of polarization. This is visible in Figure 5.3 as well as in Table 5.3 where mean values of delay spreads are presented for each case. To sum up the observations, lower delay spread values are estimated for 5.1 GHz band with both polarizations. A decrease of up to 62% in delay spread is observed for NLOS condition and up to 77% decrease for LOS condition compared with delay spread values for 2.6 GHz band. Evidently, lower delay spreads are achieved in LOS case as multipath components have lower distances to travel before they reach array than in NLOS conditions, where also more IOs are present.

5.1.4 Angle spreads of clusters

In this measurement campaign virtual very large antenna array is created with only a single antenna which is moved by the stepper motor along the array. Hence, when employing high resolution SAGE algorithm angles of arrival of MPCs are not estimated in elevation but only in azimuth angle. Consequently, vertical angle spread is not considered but only horizontal angle spread defining how spread out multipath power is about horizon. CDFs of identified cluster angle spreads, σ_φ, are presented in Figure 5.4. As expected, angle spread for different frequency bands

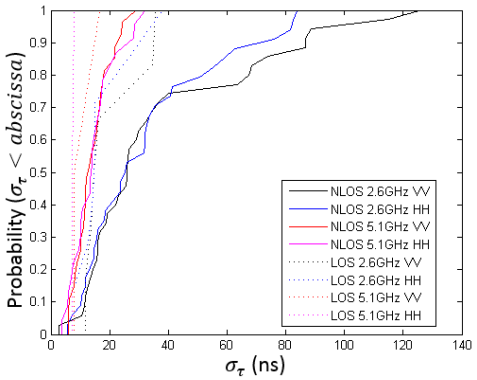

Figure 5.3: CDFs of clusters' delay spreads for both measurement frequency bands and antenna polarizations, NLOS and LOS propagation conditions.

Freq. band	2.6 GHz	2.6 GHz	5.1 GHz	5.1 GHz
Bandwidth	40 MHz	40 MHz	40 MHz	40 MHz
Polarization	VV	HH	VV	HH
NLOS				
Delay spread (ns)	38.1	33.06	14.23	14.66
LOS				
Delay spread (ns)	21.13	18.58	4.88	2.96

Table 5.3: Mean values of delay spreads for both frequency bands, polarizations, in NLOS and LOS conditions.

and polarizations are lower in LOS case than in NLOS. Impact of frequency band is evident as higher values of angle spreads are received at 2.6 GHz band. However, significant impact is observed only in LOS case whereas difference between angle spreads for both frequency bands in NLOS case is minimal. This is also confirmed in Table 5.4 where mean values of angle spreads are presented for each case. Both mean angle spread values presented in the table and CDFs of angle spreads suggest that effect of polarization on angle spread is negligible. To conclude, lower angle spread values are achieved for 5.1 GHz band with both polarizations.

5.1.5 Shadowing factor

Based on propagation environment, density of IOs between transmitter and receiver may vary. IOs appearing between transmitter and receiver might absorb some of the power of transmitted signal and scatter/reflect the rest of it. Clusters of MPCs in such environments undergo large-scale fading/shadowing. This experienced cluster power deviation from the linear regression line can be defined as cluster shadowing factor. The observed standard deviations of cluster

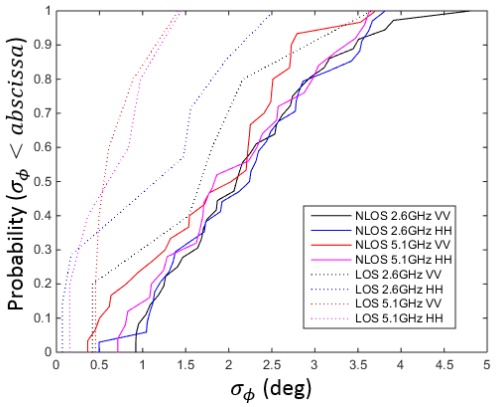

Figure 5.4: CDFs of clusters' angle spreads for both measurement frequency bands and antenna polarizations, NLOS and LOS propagation conditions.

Freq. band	2.6 GHz	2.6 GHz	5.1 GHz	5.1 GHz
Bandwidth	40 MHz	40 MHz	40 MHz	40 MHz
Polarization	VV	HH	VV	HH
NLOS				
Angle spread (deg)	2.21	2.20	1.86	2.09
LOS				
Angle spread (deg)	1.92	1.23	0.77	0.75

Table 5.4: Mean values of angle spreads for both frequency bands, polarizations, NLOS and LOS conditions.

shadowing,σ_{Shf}, are presented in Table 5.5. For 5.1 GHz band, shadowing factor is lower than for 2.6 GHz band in both NLOS and LOS conditions. Results in the table also show that effect of polarization is not substantial as considerably close shadowing factor values are achieved for both polarizations. Lower shadowing is experienced in LOS conditions than in NLOS conditions for 5.1 GHz frequency band with both polarizations. On the other hand, shadowing has higher values in LOS condition than in NLOS for 2.6 GHz band for both polarizations. As it is seen in Figure 4.2b, most of the power is contributed at the beginning of the array and there is a power attenuation over the rest array elements.

5.1.6 Cluster parameter correlation

Measurement results display that estimated delay spreads (Table 5.3) and angle spreads (Table 5.4) are considerably related. Both angle delay and angle spreads are higher in NLOS conditions and decrease in LOS conditions. It is also observed that both delay spread and angle spread achieve higher values for 2.6 GHz

Freq. band	2.6 GHz	2.6 GHz	5.1 GHz	5.1 GHz
Bandwidth	40 MHz	40 MHz	40 MHz	40 MHz
Polarization	VV	HH	VV	HH
NLOS				
σ_{Shf} (dB)	3.95	4.51	2.57	2.15
LOS				
σ_{Shf} (dB)	6.70	6.66	1.78	2.08

Table 5.5: Mean values of cluster shadowing factor for both frequency bands, polarizations, NLOS and LOS conditions.

band and lower for 5.1 GHz band. Here, weak positive correlation, $\rho_{\tau,\varphi}$, is observed between delay and angle spreads. Mean values of correlation between these two parameters are presented in rows 1 and 4 of Table 5.6. With increasing delay spread angle spread is also increasing and contrarily when delay spread decreases so does the angle spread. CDFs of angle spread and delay spread correlation for each band, polarization and propagation condition are illustrated in Figure 5.5a.

There is correlation identified between angle spread and delay spread however, cluster angle spread and delay spread show low correlation with cluster shadowing. It is visible in rows 2 and 5 of Table 5.6 that almost for all cases correlation between delay spread and shadowing is weak negative and reaches up to -0.36 (2.6 GHz band with VV polarization in NLOS condition). For LOS conditions correlation values are closer to zero but standard deviation of delay spread and shadowing correlation is about 0.2. On the other hand, no significant difference is evident between different polarizations. CDFs of delay spread and shadowing are illustrated in Figure 5.5b. Negative correlation between delay spread and shadowing indicates that with weaker signal, the delay spread increases, and when received signal is relatively strong delay spread decreases.

Rows 3 and 6 of Table 5.6 show, that correlation between angle spread and shadowing is very low, equal to zero and negative. No (0) or very low (0.02) correlation is observed for 5.1 GHz band with VV polarization in NLOS and LOS conditions, respectively. However, estimated standard deviation of angle spread and shadowing correlation is about 0.21 and 0.22 for NLOS and LOS conditions respectively. Low negative correlation can be seen for 5.1 GHz band with HH polarization (-0.10 in NLOS conditions and -0.27 in LOS conditions). Very low (0.06 in LOS conditions with VV polarization) and low negative (-0.24 in NLOS conditions with VV polarization) correlation is achieved for 2.6 GHz band. Standard deviation of correlation for this case is 0.26 and 0.4 for NLOS and LOS respectively. CDFs of angle spread and shadowing are presented in Figure 5.5c. With higher shadow loss, angle spread is increasing.

Mean estimated correlation values between parameters listed in Table 5.6 are weak or very weak. However, as it is visible in the Figure 21 for some cases correlation values span from almost -1 up to 0.8. Also given standard deviations of correlations indicate the spread of distribution. Therefore, estimated correlation values should not be ignored.

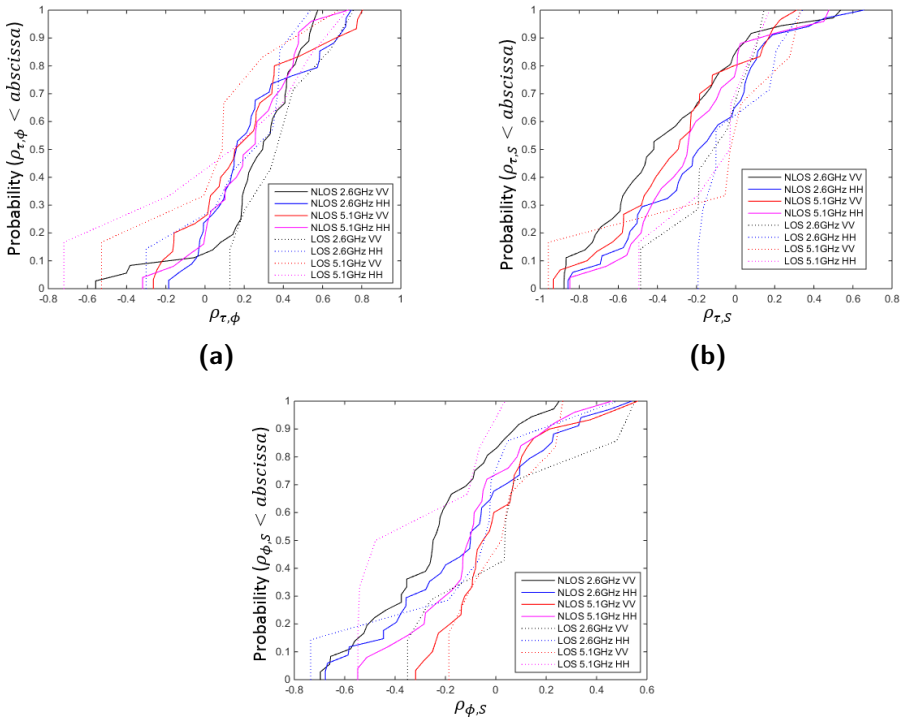

Figure 5.5: CDFs of clusters' correlation between (a) angle spread and delay spread, (b) delay spread and shadowing, (c) angle spread and shadowing, for both frequency bands, polarizations, NLOS and LOS conditions.

Freq. band	2.6 GHz	2.6 GHz	5.1 GHz	5.1 GHz
Bandwidth	40 MHz	40 MHz	40 MHz	40 MHz
Polarization	VV	HH	VV	HH
NLOS				
$\rho_{\tau,\varphi}$	0.25	0.25	0.18	0.21
$\rho_{\tau,S}$	-0.36	-0.17	-0.30	-0.24
$\rho_{\varphi,S}$	-0.24	-0.11	0.00	-0.10
LOS				
$\rho_{\tau,\varphi}$	0.37	0.22	0.11	0.15
$\rho_{\tau,S}$	-0.10	0.02	-0.07	-0.08
$\rho_{\varphi,S}$	0.06	-0.11	0.02	-0.27

Table 5.6: Mean values of clusters' correlation between different parameters for both frequency bands, polarizations, NLOS and LOS conditions.

5.2 Impact of antenna directivity

5.2.1 Number of clusters

Based on antenna radiation directivity basically all antennas can be classified as isotropic and directional. When coverage is required in all directions around transmitter with respect to the antenna orientation omni-directional antennas with 360 degree horizontal radiation pattern can be employed. For considerably complex environment containing a number of IOs, use of omni-directional antenna may result in high multipath richness. Unlike with directional antenna signal transmitted from omni-directional antenna encounters more IOs in the environment and can undergo propagation mechanisms leading to moderate or complete obstruction, or scattering. Thus, after propagation mechanisms ordinarily more clusters of MPCs are present which is confirmed in rows 1 and 3 of Table 5.7 where mean numbers of clusters, N_c, are presented for omni-directional and directional antenna configurations. In both conditions, when MS is in NLOS and LOS in respect to the receiving antenna array, higher N_c is obtained with omni-directional antennas. For omni-directional antenna in LOS conditions N_c is lower than in NLOS as most of the MPCs are the contributions of LOS component and relatively strong reflections from the walls close to antenna array. This is confirmed by dynamic range of the clusters which is shown in rows 2 and 4 of Table 5.7. The ratio of strongest and weakest observed clusters has bigger value in NLOS than in LOS. With omni-directional antennas the power is radiated in all horizontal directions. However, with the big number of clusters their power contributions might be lower compared to the clusters' of MPCs' when power is radiated into particular direction using directive antenna. Rows 2 and 4 of Table 5.7 show that dynamic range in NLOS condition for directive antenna is lightly lower than for omni-directional but it is higher in LOS condition. Such comparably big dynamic range for directional antenna is caused by the presence of very strong LOS contribution and contribution of smaller clusters with low total power. It has to be noted that N_c for each case is found after elimination of weak clusters using a 20 dB threshold for NLOS and 30 dB threshold for LOS as it was done in previous chapter.

Freq. band	2.6 GHz	2.6 GHz
Antenna directivity	Omni-directional	Directional
NLOS		
N_c	37	15
Dynamic range (dB)	22.52	20.74
LOS		
N_c	32	25
Dynamic range (dB)	14.79	43.16

Table 5.7: Number of clusters and dynamic range for omni-directional and directive antennas, in NLOS and LOS conditions.

5.2.2 Observed length and visibility gain of clusters

Observed lengths of clusters over the antenna array vary for both types of antennas. Distribution of observed cluster lengths in meters for NLOS and LOS conditions are illustrated in Figure 5.6a and Figure 5.6b. In NLOS conditions most of the clusters are up to around 4 meters length. There is only one cluster with observed BS-VR of around 7 meters. It is considered as reflection from the wall in front of the antenna array. The rest of the clusters for NLOS conditions with shorter observed BS-VRs are contributions of different IOs in the environment. Similar distribution of observed BS-VRs is in LOS conditions (Figure 5.6b). Fewer clusters are observed, however, most of them are also up to around 4 meters length. There is also only one cluster of around 7 meters length visible to the array for omni-directional and directional antennas. This cluster is considered as LOS component when MS is visible to the antenna array. The reflection from the wall on the left side of the array which is also a significant contributor is not visible over the entire array as it is stronger only at the last window positions. This contributor is considered as second longest observed cluster. The rest of the clusters are contributions from propagation mechanisms mainly from the walls of the buildings near antenna array and somewhat from other IOs in the environment. Figure 5.6 also illustrates that more clusters are observed with omni-directional antenna than with directional as it was mentioned in previous chapter.

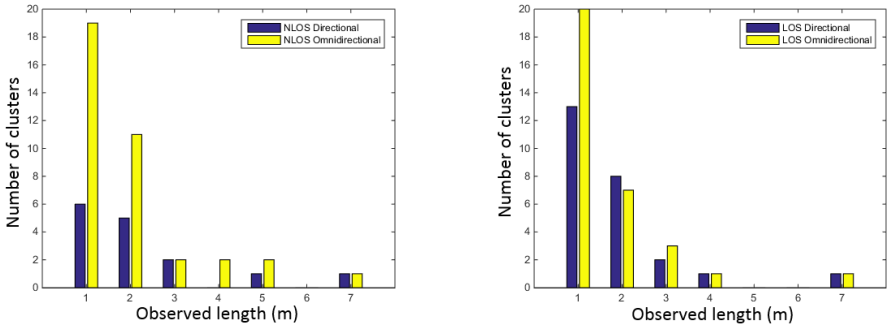

(a) **(b)**

Figure 5.6: Observed length of clusters in meters for NLOS (a) conditions and LOS (b) conditions.

Power variation over the observed BS-VR is present for each identified cluster because of non-stationary phenomenon for very large antenna arrays. Mean values of the slope of the linear regression defining the power variation of the cluster are presented in Table 5.8. Higher slopes in dB/m are characteristic for omni-directional antennas than for directive antennas in both LOS and NLOS conditions. However, values are quite small and close to zero. This is also visible in CDFs of slopes for both antennas that are illustrated in Figure 5.7.

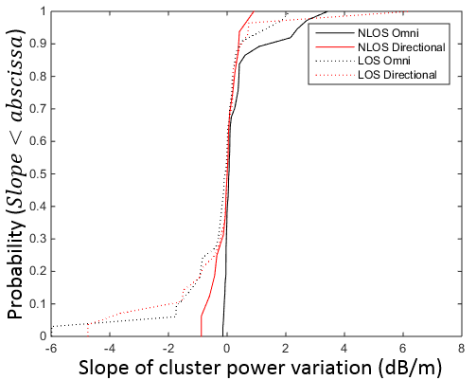

Figure 5.7: Slopes of cluster power variations for omni-directional and directive antennas, in NLOS and LOS conditions.

Freq. band Antenna directivity	2.6 GHz Omni-directional	2.6 GHz Directional
NLOS Slope (dB/m)	0.39	-0.01
LOS Slope (dB/m)	-0.29	-0.17

Table 5.8: Mean values of the slopes for omni-directional and directive antennas, in NLOS and LOS conditions.

5.2.3 Delay spreads of clusters

Delay spread, σ_τ, for each cluster is calculated for omni-directional and directional antennas using equations 4.2–4.4. Table 5.9 shows clear difference between values achieved when MS is in LOS and in NLOS. Delay spreads of clusters reach higher values in NLOS conditions than in LOS due to multipath richness and larger distances between transmitter and receiver. This is also visible in CDFs of delay spreads illustrated in Figure 5.8. Delay spread values for both antenna setups are very similar in both LOS and NLOS conditions. However, slightly higher values are achieved for directional antenna which indicates that received energy is a bit more spread out in time. The observed delay spread appears from multipath reflections and scattering in the propagation environment which cause increased delays with strong signals. In some cases misalignment of transmitter and receiver antenna can also supplement to increase of delay spread for directional antenna. In this measurement campaign receiving antenna array was positioned on the three-story building while transmitting antenna was on the parking lot besides the building.

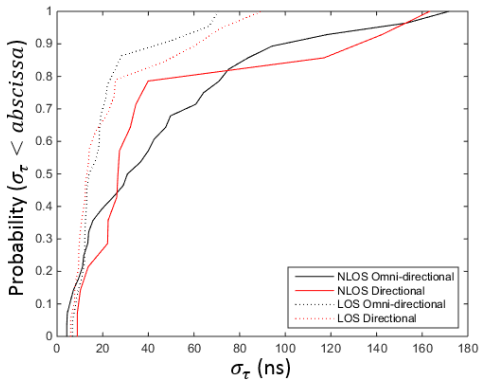

Figure 5.8: CDFs of clusters' delay spreads for omni-directional and directive antennas, in NLOS and LOS conditions.

Freq. band	2.6 GHz	2.6 GHz
Antenna directivity	Omni-directional	Directional
NLOS		
Delay spread (ns)	46.78	49.04
LOS		
Delay spread (ns)	21.83	24.79

Table 5.9: Mean values of delay spreads for omni-directional and directive antennas, in NLOS and LOS conditions.

5.2.4 Angle spreads of clusters

In this measurement campaign only azimuth angles of arrival are estimated using SAGE algorithm for both antenna setups. Angle spread, σ_φ, of clusters then can be calculated using Equation 4.5. Figure 5.9 illustrates how spread out multipath power is about horizon. Angle spread for omni-directional antenna is visibly higher than for directional antenna. In the environment full of scatterers directional antennas radiate energy in set direction, therefore, avoiding interaction with some IOs. At the same time directional antenna at the receiver is able to catch most of the transmitted energy. However, mean angle spread values in Table 5.10 suggest that the difference for omni-directional and directional antennas is not significant. Low differences are also observed for angle spread values in NLOS and LOS conditions.

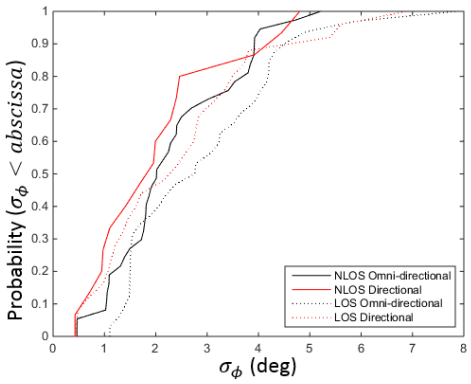

Figure 5.9: CDFs of clusters' angle spreads for omni-directional and directive antennas, in NLOS and LOS conditions.

Freq. band Antenna directivity	2.6 GHz Omni-directional	2.6 GHz Directional
NLOS Angle spread (deg)	2.35	2.10
LOS Angle spread (deg)	2.97	2.52

Table 5.10: Mean values of angle spreads for omni-directional and directive antennas, in NLOS and LOS conditions.

5.2.5 Shadowing factor

Large-scale fading/shadowing over the large antenna array is described as power variations due to IOs obstructing propagation path between transmitter and receiver. Mean values of cluster power deviations from the linear regression line for omni-directional and directional antennas are presented in Table 5.11. Somewhat higher shadowing factor, σ_{Shf}, is achieved for omni-directional antenna. However, difference is quite small. For omni-directional antenna, σ_{Shf} is bigger by 0.7 dB in NLOS conditions and 0.29 dB in LOS conditions than for directional antenna. Shadowing factor has slightly higher values in LOS conditions than in NLOS conditions for both antenna setups.

Freq. band Antenna directivity	2.6 GHz Omni-directional	2.6 GHz Directional
NLOS σ_{Shf} (dB)	3.64	2.94
LOS σ_{Shf} (dB)	4.35	4.06

Table 5.11: Mean values of shadowing factor for omni-directional and directive antennas, in NLOS and LOS conditions.

5.2.6 Cluster parameter correlation

Table 5.12 shows mean values of correlation between cluster delay spread and angle spread, delay spread and shadowing, angle spread and shadowing, for omni-directional and directional antennas in LOS and NLOS conditions. Results in rows 1 and 4 of Table 5.12 show that angle spread and delay spread of cluster are related. Thus, weak positive correlation $\rho_{\tau,\varphi}$ is observed between described parameters in both LOS and NLOS conditions. Clusters with low delay spread also have low angle spread and cluster with higher angle spread have also a higher delay spread. Values of $\rho_{\tau,\varphi}$ are rather similar for omni-directional and directional antennas in LOS and NLOS conditions. Slightly higher correlation is observed for omni-directional antenna. CDFs of angle spread and delay spread correlation are illustrated in Figure 5.10a.

Rows 2 and 5 of Table 5.12 show that cluster delay spread and shadowing have low-negative correlation, $\rho_{\tau,S}$, for both omni-directional and directional antennas. Correlation between parameters is also similar for both propagation conditions. Standard deviation between delay spread and shadowing correlation is around 0.5. For the strong signal the delay spread is reduced and for a weak signal delay spread increases. CDFs of delay spread and shadowing correlation are presented in Figure 5.10b.

Rows 3 and 6 of Table 5.12 indicate that shadowing has also low-negative correlation with angle spread. Correlation for omni-directional and directional antennas is similar in NLOS as well as in LOS conditions. Standard deviation of angle spread and shadowing correlation is around 0.3 for NLOS and 0.4 for LOS conditions. For negative correlation with higher shadow loss, angle spread is also higher. CDFs of angle spread and shadowing are presented in Figure 5.10c.

Figure 5.10 as well as estimated standard deviations of correlations indicate that even if the mean correlation values are relatively low they still should be considered. Figure 5.10 illustrates correlation values spanning from around -1 to 1 while standard deviation of correlation reaches up to 0.5 showing the spread distribution of estimated correlations.

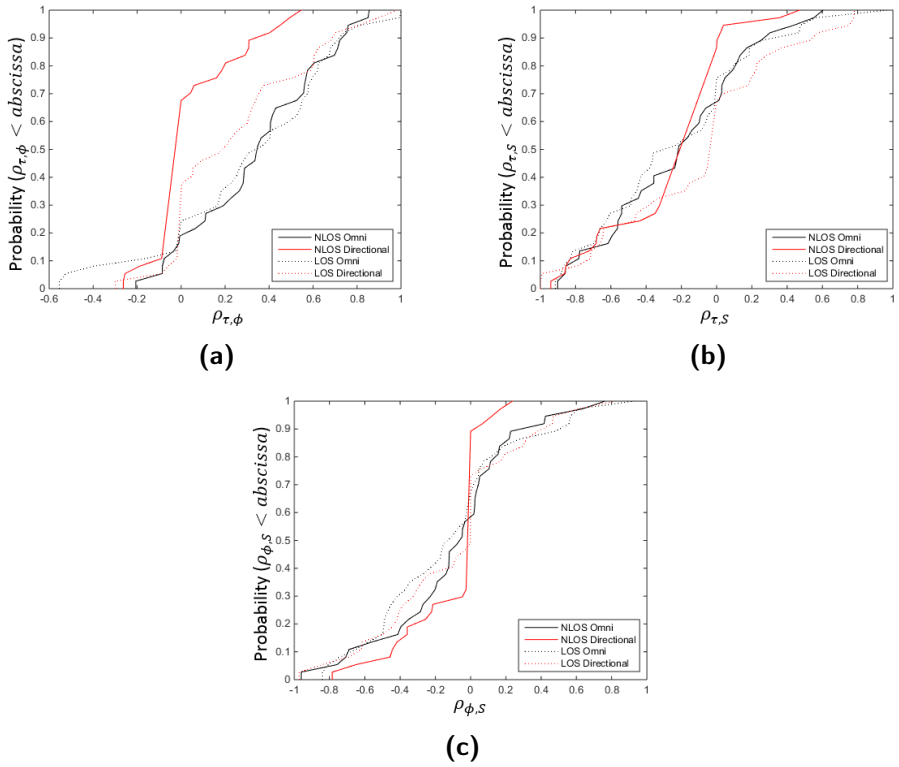

Figure 5.10: CDFs of clusters' correlation between (a) angle spread and delay spread, (b) delay spread and shadowing, (c) angle spread and shadowing, for omni-directional and directive antennas, in NLOS and LOS conditions.

Freq. band Directivity	2.6 GHz Omni-directional	2.6 GHz Directional
NLOS		
$\rho_{\tau,\varphi}$	0.35	0.17
$\rho_{\tau,S}$	-0.21	-0.40
$\rho_{\varphi,S}$	-0.09	-0.32
LOS		
$\rho_{\tau,\varphi}$	0.37	0.33
$\rho_{\tau,S}$	-0.25	-0.12
$\rho_{\varphi,S}$	-0.14	-0.13

Table 5.12: Mean values of clusters' correlation between different parameters for omni-directional and directive antennas, in NLOS and LOS conditions.

Chapter 6
Summary

The aim of this thesis work is to study the effect of frequency band, antenna polarization, and antenna directivity, on the channel properties of massive MIMO systems. Channel measurement campaign using very large antenna array in base station is conducted in order to collect data. MPCs are then extracted from the measurement data using SAGE algorithm. Groups of extracted MPCs characterized by similar parameters — propagation delay, azimuth angle-of-arrival, and complex power — are seen as clusters which are identified using sequential delay-angular visual clustering method. Visual cluster identification is chosen based on the fact that measurement environment is well known and thus clusters may be related to the IOs present between transmitter and receiver. Impact of frequency band, antenna polarizations and directivity on resulting clusters' parameters is then studied.

Identified clusters for 2.6 GHz band and 5.1 GHz band with both vertical/vertical and horizontal/horizontal antenna polarizations are related to the same IOs in the environment. Similar results are achieved using omni-directional antenna, however, more clusters are identified. There was no significant impact of antenna polarization observed for all estimated parameters. Mean cluster delay spreads (from 3 ns to 49 ns) for all frequency bands, polarizations, antenna directivities are not very large. Lower cluster delay spreads and angle spreads are observed for 5.1 GHz band than for 2.6 GHz. For antenna directivity comparison similar results are achieved using both antenna configurations. Delay spread is slightly lower when using omni-directional antenna, however, angle spread and shadowing factor are higher than with directional antenna. Shadowing factor is also achieved higher for 2.6 GHz band than for 5.1 GHz band. Clearly, lower delay spread values of estimated cluster parameters are achieved in LOS conditions than in NLOS conditions.

Positive correlation between angle spread and delay spread are estimated while correlation between spreads and shadowing is negative. Similar values are achieved for both investigated frequency bands with both polarizations. There is also no distinct difference between omni-directional and directional antennas. Estimated mean correlation values are low or very low, however, presented CDFs and standard deviations of correlations indicate the spread distribution of estimated correlations.

Modeling of cluster parameters and their correlations estimated in this thesis work may enable channel models to reflect the characteristics demonstrated by real

wireless communication channels under different wireless system configurations.

References

[1] F. Rusek, D. Persson, Buon Kiong Lau, E.G. Larsson, T.L. Marzetta, O. Edfors, F. Tufvesson, "Scalling Up MIMO: Opportunities and Challenges with Very Large Arrays", *IEEE Signal Processing Magazine*, vol.30, issue 1, pp.40–60, ISSN 1053-5888,Jan 2013.

[2] E.G. Larsson, O. Edfors, F.Tufvesson, T.L. Marzetta, "Massive MIMO for Next Generation Wireless Systems", *IEEE Communications Magazine*, vol.52, issue 2, pp.186–195, ISSN 0163-6804, Feb 2014.

[3] X. Gao, O. Edfors, F. Rusek, F. Tufvesson, "Massive MIMO Performance Evaluation Based on Measured Propagation Data", *Wireless Communications, IEEE Transactions on*, vol.14, issue 7, pp.3899–3911, ISSN 1536-1276, Mar 2015.

[4] X. Gao, F. Tufvesson, O. Edfors, F. Rusek, "Measured propagation characteristics for very-large MIMO at 2.6 GHz", in the *Signals, Systems and Computers (ASILOMAR), 2012 Conference Record of the Forty Sixth Asilomar Conference on* pp.295–299, ISBN 978-1-4673-5050-1, Pacific Grove, CA, USA, Nov 2012.

[5] X. Gao, F. Tufvesson, O. Edfors, "Massive MIMO channels — Measurements and Models", in the *Signals, Systems and Computers, 2013 Asilomar Conference on* pp.280–284, ISBN 978-1-4673-5050-1, Pacific Grove, CA, USA, Nov 2013.

[6] X. Gao, O. Edfors, F. Rusek, F. Tufvesson, "Massive MIMO in Real Propagation Environmnets", *IEEE Transactions on Wireless Communications, 2015*, Jul 2015.

[7] S. Payami, F. Tufvesson, "Delay Spread Properties in Measured Massive MIMO systems at 2.6 GHz", in the *Personal Indoor and Mobile Radio Communications (PIMRC), 2013 IEEE 24th International Symposium on*, pp.53–57, ISSN 2166-9570, London, UK, Sept 2013.

[8] A. F. Molisch, *Wireless communications*, Second edition, John Wiley & Sons Ltd, ISBN 978-0-470-74186-3, 2011.

[9] D. K. Cheng, *Fundamentals of Engineering Electromagnetics*, Prentice Hall, ISBN 9780201566116, 1992.

[10] Pajusco, P., Malhouroux-Gaffet, N., El Zein, G., "Comprehensive Characterization of the Double Directional UWB Residential Indoor Channel", *Antennas and Propagation, IEEE Transactions on*, vol.63, issue 3, pp.1129–1139, ISSN 0018-926X, London, UK, Jan 2015.

[11] L. Schumacher, L. T. Berger, and J. Ramiro-Moreno, "Recent advances in propagation characterization and multiple antenna processing in the 3GPP framework", *in the 3GPP framework,in Proceedings of XXVIth URSI General Assembly*, 2002.

[12] W. Weichselberger, M. Herdin, H. Ozcelik, E. Bonek, "A Stochastic MIMO Channel Model with Joint Correlation of Both Link Ends", *IEEE Trans. on Wireless Comm*, vol.5, issue 1, pp.90–100, Jan 2006.

[13] Nelson Costa, Simon Haykin, Ernst Bonek, *Multiple-Input Multiple-Output Channel Models: Theory and Practice*, John Wiley & Sons Ltd, ISBN 978-0-470-39983-5, April 2010.

[14] H. Hofstetter, G. Steinbock, "A geometry based stochastic channel model for MIMO systems", *Smart Antennas, 2004. ITG Workshop on*, pp.194–199, ISBN 0-7803-8327-3, Mar 2004.

[15] K. Haneda, J. Poutanen, F.Tuvfesson, L. Lingfeng, V. Kolmonen, P. Vainikainen, C. Oestges, "Development of multi-link geometry-based stochastic channel models", in the *Antennas and Propagation Conference (LAPC), 2011 Loughborough*, pp.1–7, ISBN 978-1-4577-1014-8, Loughborough, UK, Nov 2011.

[16] L. Liu, C. Oestges, J. Poutanen, K. Haneda, P. Vainikainen, F. Quitin, F. Tufvesson, P.D. Doncker, "Development of multi-link geometry-based stochastic channel models", *Wireless Communications, IEEE*, vol.19, issue 6, pp.92–99, ISSN 1536-1284, Dec 2012.

[17] S. Payami, F. Tufvesson, "Channel measurements and analysis for very large array systems at 2.6 GHz", in the *Antennas and Propagation (EUCAP), 2012 6th European Conference on*, pp.433–437, ISBN 978-1-4577-0918-0, Prague, Czech rep., Mar 2012.

[18] X. Gao, F. Tufvesson, F. Rusek, O. Edfors, "Linear Pre-Coding Performance in Measured Very-Large MIMO Channels", in the *Vehicular Technology Conference (VTC Fall), 2011 IEEE*, pp.1–5, ISBN 978-1-4244-8328-0, San Francisco, CA, USA, Sept 2011.

[19] M. Gauger, J. Hoydis, C. Hoek, H. Schlesinger, A. Pascht, S. Brink, "Linear Pre-Coding Performance in Measured Very-Large MIMO Channels", in the *SCC 2015; 10th International ITG Conference on Systems, Communications and Coding; Proceedings of*, pp.1–6, ISBN 978-3-8007-3659-1, Hamburg, Germany, Feb 2015.

[20] Jinxing Li, Youping Zhao, "Channel characterization and modeling for large-scale antenna systems", in the *Communications and Information Technologies (ISCIT), 2014 14th International Symposium on*, pp.559–563, Incheon, South Korea, Sept 2014.

[21] A. O. Martinez, E. D. Carvalho, J. O. Nielsen, "Towards very large aperture massive MIMO: A measurement based study", in the *Globecom Workshops (GC Wkshps)*, pp.281–286, Austin, TX, USA, Dec 2014.

[22] B.H. Fleury, M. Tschudin, R. Heddergott, D. Dahlhaus, K. Ingeman Pedersen "Channel parameter estimation in mobile radio environments using the SAGE algorithm", *Selected Areas in Communications, IEEE Journal on*, vol.17, issue 3, pp.434–450, ISSN 0733-8716, Aug 2002.

[23] B.H. Fleury, X. Yin, K.G. Rohbrandt, P. Jourdan, A. Stucki, "Performance of a High-Resolution Scheme for Joint Estimation of Delay and Bidirection Dispersion in the Radio Channel", in the *Vehicular Technology Conference, 2002. VTC Spring 2002. IEEE 55th*, pp.522–526, ISBN 0-7803-7484-3, 2002.

[24] S. Wu, C-X Wang, E.H.M.Aggoune, M.M. Alwakeel, Yejun He, "A Non-Stationary 3-D Wideband Twin-Cluster Model for 5G Massive MIMO ChannelsâĂİ, Selected Areas in Communications", *Selected Areas in Communications, IEEE Journal on* , vol.32, issue 6, pp.1207–1218, ISSN 0733-8716, 2014.

[25] G.D. Durgin, *Space-Time Wireless Channels*, New Jersey, USA, Prentice Hall, ISBN 0-13-065647-X, 2003.

[26] M. Ibnkahla, *Signal Processing for Mobile Communications Handbook*, CRC Press, ISBN 978-0849316579, Aug 2004.

[27] N. Czink, E. Bonek, L. Hentila, P. KyÃűsti, J-P Nuutinen, J. Ylitalo, "The Interdependence of Cluster Parameters in MIMO Channel Modelling", in the *Antennas and Propagation, 2006. EuCAP 2006. First European Conference on*, pp.1–6, ISBN 978-92-9092-937-6, Nice, France, Nov 2006.

[28] G. S. Dahman, R. J. C. Bultitude, R. H.M. Hafez, "Identifying and Modelling Multipath Clusters in Propagation Measurement Data", in the *Vehicular Technology Conference Fall (VTC 2010-Fall), 2010 IEEE 72nd*, pp.1–5, ISBN 978-1-4244-3573-9, Ottawa, ON, Canada, Sept 2010.

[29] C. Schneider, M. Ibraheam, S. Hafner, M. Kaske, M. Hein, R.S. Thomas, "Identifying and Modelling Multipath Clusters in Propagation Measurement Data", in the *Antennas and Propagation (EuCAP), 2014 8th European Conference on*, pp.449–453, The Hague, Netherlands, Apr 2014.

[30] A. A. M. Saleh, R. A. Valenzuela, "A statistical model for indoor multipath propagationâĂİ, Selected Areas in Communications", *Selected Areas in Communications, IEEE Journal on*, vol.5, issue 2, pp.128–137, ISSN 0733-8716, Jan 2003.

[31] L. Vuokko, V.M. Kolmonen, J. Salo, P. Vainikainen, "Measurement of Large-Scale Cluster Power Characteristics for Geometric Channel Models", *Antennas and Propagation, IEEE Transactions on*, vol.55, issue 11, pp.3361–3365, ISSN 0018-926X, Nov 2007.